

Removal of As (V) in water using β -Cyclodextrin intercalated Fe-Al layered double hydroxide/reduced Graphene Oxide nanocomposites

V. Nithya Priya, M. Rajkumar^{*}, J. Mobika, S.P.Linto Sibi

Department of Physics, PSG College of Arts and Science, Coimbatore - 641 014, India

ARTICLE INFO

Keywords:

Layered double Hydroxide
 β -cyclodextrin
Reduced Graphene oxide
As (V) adsorption

ABSTRACT

Highly effective nanoadsorbent based on β -Cyclodextrin intercalated Fe-Al layered double hydroxide/reduced Graphene Oxide (FAH-rGO/CD) nanocomposites were synthesized through hydrothermal and *ex-situ* polymerization process for As (V) adsorption in wastewater. Characterization results of XRD, FESEM and HRTEM reveals the crystalline structure and morphology of the FAH-rGO/CD nanocomposites. The elemental composition and functional groups of the composites were investigated by EDS and FTIR. N_2 adsorption-desorption analysis was utilized to determine the surface area of the prepared nanocomposite and the incorporated β -CD moieties enhances the surface area of FAH-rGO ($145.35 \text{ m}^2 \text{ g}^{-1}$). Various adsorption parameters of nanoadsorbents such as the effect of pH, contact time, adsorbent dosage, adsorption isotherms and kinetics were studied and reported. The obtained adsorption isotherm data of synthesized adsorbent was properly fitted with Langmuir isotherm model along with their maximum monolayer adsorption capacity of 185.52 mg g^{-1} for As (V). The Pseudo-first and second kinetic models were used to assess the kinetic data and the adsorption of As (V) pursued the Pseudo second order model with high correlation co-efficient R^2 value (0.9836). Moreover, as-synthesized adsorbents had good recyclability up to 89%, even after five adsorption-desorption analysis. Meanwhile, the presence of co-existing anions on sorption of As (V) was evaluated and their results indicate that, the high concentration of phosphate and carbonate ions inhibited the efficiency of As (V) removal. Thus, high surface area with abundant oxygen containing hydroxyl groups and magnetic properties of FAH-rGO/CD nanocomposites proved to be highly effective adsorbent for As (V) removal in wastewater.

1. Introduction

In heavy metals, Arsenic (As) is considered as the most abundant, destructive and the virulent element present in water bodies and it serves as a major threat to the human beings and the ecosystem as it accumulates in the food chain. Generally, the oxidation state of arsenic species describes the toxicity level of arsenic in aqueous medium [1,2]. The primary forms of inorganic arsenic species (e.g. arsenite (As (III) and arsenate (As (V)) is considered as the most vulnerable compared to the other organic species (e.g. monomethyl and dimethyl arsenic acid (MMAA & DMAA), and arseno-sugars) owing to their highly toxic and carcinogenic nature towards human health. Some of the previous researches have declared that, As (V) species that occurs in aerobic water surface has better removal efficiency than As (III) species in anaerobic water surface and it could be possibly oxidized to convert as As (V) by strong oxidizing agents. Therefore, it is more comfortable to examine the presence of As (V) ions to be removed in drinking water [3–5]. Based on

the toxicity of arsenic species and guidelines for drinking water quality, World Health Organization (WHO) has reduced the contamination level of arsenic in drinking water as 0.01 mg/L from 0.05 mg/L [6,7]. To diminish the arsenic contamination in water, various wastewater treatments are followed such as precipitation [8], oxidation [9], liquid-liquid extraction [10], surface complexation [11], membrane process [12], ion-exchange membrane [13,14] and selective adsorption [4,15–26]. Among these wastewater treatments, the adsorption has attained more attention because of their advantages such as high removal capacity of the adsorbent, cost-effectiveness, simple and prompt process and their easy handle etc., [27–33]. In various adsorbents, more priority is given to magnetic-based adsorbents as it would have adequately large surface area and are easy to separate with an exterior magnetic field. Their advantages overcome the difficulties normally associated with other bio-polymeric adsorbents [34].

β -cyclodextrin is categorized as cyclic oligosaccharide which consists of seven D-glucose units connected through α -(1–4) linkages along with

^{*} Corresponding author.

E-mail address: vmanirajkumar@gmail.com (M. Rajkumar).

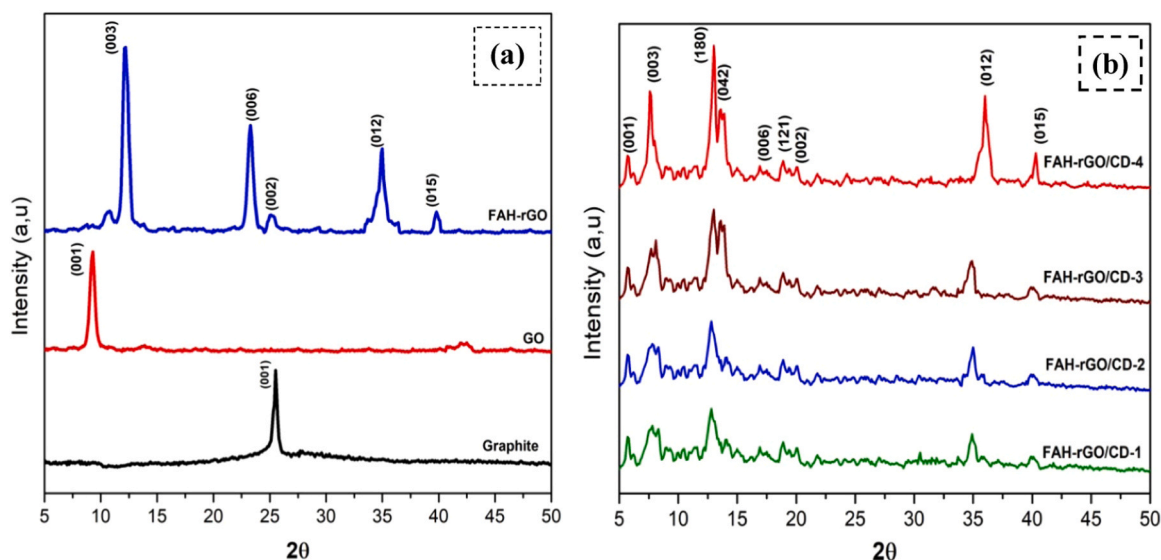


Fig. 1. (a-b) XRD patterns of graphite, GO, FAH-rGO and FAH-rGO/CD (1–4).

unique hydrophobic inner cavity and outer hydrophilic environment. It exhibits the structure of torus-shaped ring which consists of a polar cavity with a primary hydroxyl group lying on external surfaces and secondary hydroxyl group in internal surface. The biodegradable and renewable CD molecules have the capability to combine various organic and inorganic compounds selectively through their cavities. These form stable host-guest inclusion complexes using various interactions such as Van der Waals, dipole-dipole interactions and hydrogen bonding. Through the β -CD/metal complexes, arsenic species can easily make complexes with polar hydroxyl functional groups of β -cyclodextrin and it can also promote the solubility of pollutants, reduce the toxicity and catalyze the decomposition. Due to weak mechanical strength and low surface area of bio-sorbent, it's not easy to separate them from liquid phase which hindered their application in wastewater treatment. To overcome these defects of bio-sorbent, it's highly preferable to develop new adsorbent with high surface area, high adsorption capacity and ability to ease the separation [34–36].

Depending upon these concerns, Graphene oxide (GO) has been chosen as one of the functionalized material with β -CD because of their unique properties such as large surface area and high mechanical strength and it could be considered as the best promising material to possess high adsorption capacity along with the huge number of active sites [20,24,34]. Basically, Graphene oxide contains the more number of active sites like epoxy, hydroxyl and carboxylic groups on their surfaces and edges to significantly promote the rate of adsorption [37–41]. On the other side, layered double hydroxide (LDH) with magnetic properties has established relatively high surface area with hydroxyl functional groups on their surface. These adsorb heavy metals and can be easy to separate with an exterior magnetic field. It has excellent adsorption capacity to adsorb heavy metal ions through ionic interaction and classifies as anionic clay. General formula for LDH is $[M^{2+}_{1-x}M^{3+}_x(OH)_2]^{x+}[(A^{n-})_{x/n} \cdot mH_2O]$, where M^{2+} , M^{3+} are denote the cations of metal ions such as Fe^{2+} and Al^{3+} , while A^{n-} represents the interlayer anions. In LDH, M^{2+} ions are octahedrally restructured by replacing M^{3+} ions through the hydroxyl groups which results in negatively charged metal hydroxide. Various numbers of metal groups in LDH such as M^{2+} , M^{3+} and A^- have generated the largest number of isostructural materials with varying physical and chemical properties. Hereby, the influences of metal hydroxide in LDH have been mainly used to adsorb the heavy metals [4,42–47].

However, few studies have investigated the use of various LDH/GO/

β -CD adsorbents such as Graphene oxide/ferric hydroxide [15], Magnetite-partially reduced graphene oxide [48], Zn/Fe-LDH microspheres [49], Magnetite-graphene-LDH [50], Magnetic nanoparticle-supported Layered double hydroxide nanocomposites [51], Cobalt-aluminum layered double hydroxide on boehmite surface [52], Magnetic nanoparticles decorated with β -cyclodextrin functionalized graphene oxide [53], Zero-valent iron impregnated chitosan carboxymethyl- β -cyclodextrin composite beads [54] for adsorption of As (V). Herein, we report β -cyclodextrin intercalated on FAH-rGO (FAH-rGO/CD) nanocomposite adsorbent for As (V) removal which can be subsequently separated from aqueous medium through the external magnetic field with high adsorption capacity and high removal efficiency and it can be reused.

However, the synthesis of β -cyclodextrin intercalated Fe-Al layered double hydroxide/reduced Graphene Oxide (FAH-rGO/CD) nanocomposite and their application for As (V) removal with high adsorption capacity have not been reported in the literature. Therefore, the main purpose of this study were: (i) to prepare and characterize the different weight percentages of β -cyclodextrin intercalated on FAH-rGO composites (ii) to examine the effect of pH, effect of contact time, effect of adsorbent dosage, adsorption isotherms and kinetics for As (V) adsorption, (iii) to study the effect of co-existing anions and further discuss the adsorption mechanism of as-synthesized adsorbent.

2. Material and methods

2.1. Chemicals

Graphite powder (G) and Beta Cyclodextrin (β -CD) were purchased from Sigma Aldrich, sodium nitrate (Na_2NO_3), potassium permanganate ($KMnO_4$), sulfuric acid (H_2SO_4 , 98%), hydrochloric acid (HCl), hydrogen peroxide (H_2O_2 , 30%), ferrous chloride ($FeCl_2 \cdot 0.4 H_2O$), aluminum chloride ($AlCl_3 \cdot 0.6 H_2O$) and ethanol (C_2H_5OH) of analytical grade, were purchased from Merck. All other chemicals were utilized for the synthesis of composites without further purification.

2.2. Synthesis of FAH-rGO

In this present work, Modified Hummer's method was followed to prepare Graphene oxide (GO) from natural graphite powder [15]. FAH-rGO composites were prepared by means of hydrothermal method as

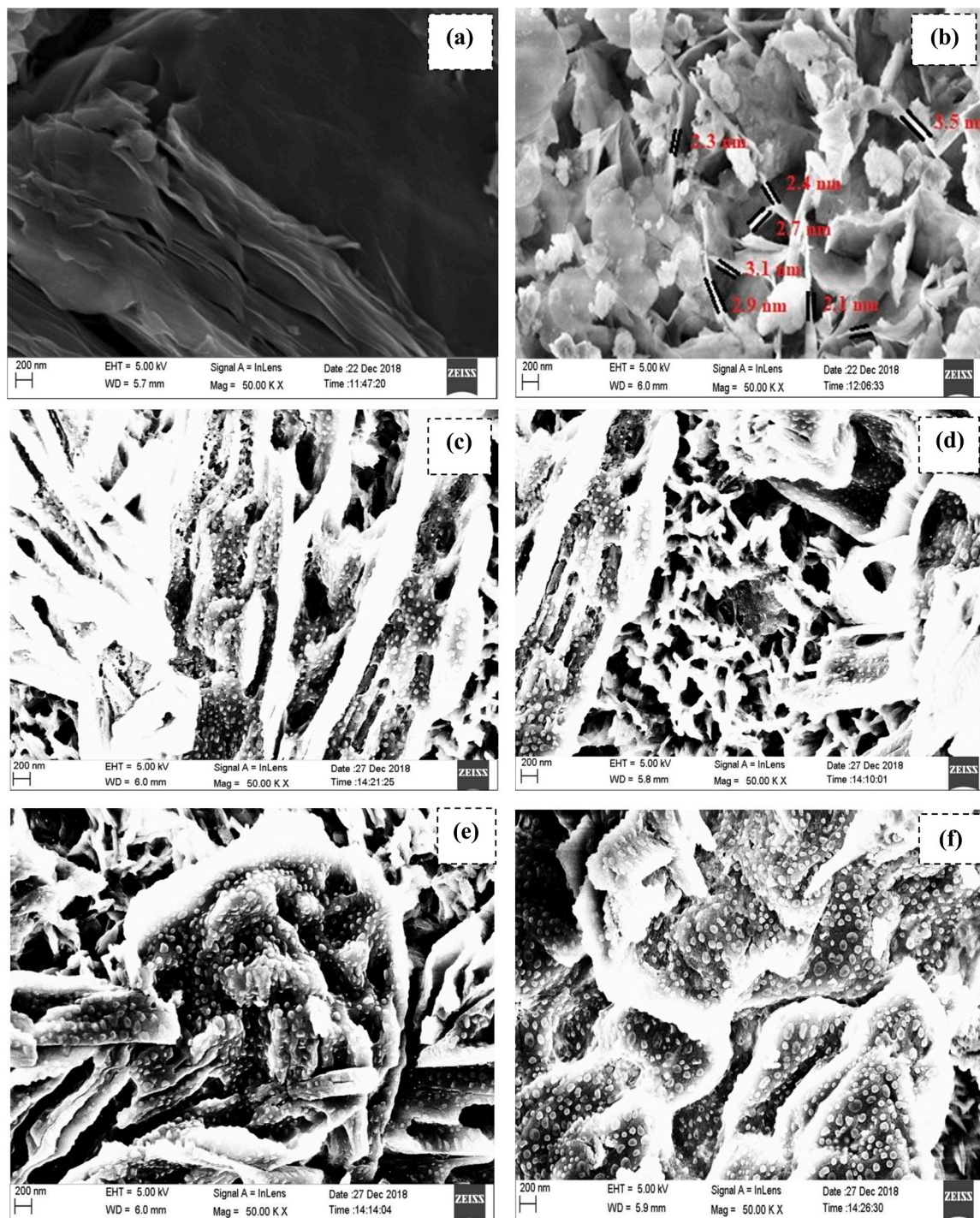


Fig. 2. (a-f) FESEM images of GO, FAH-rGO, FAH-rGO/CD-1, FAH-rGO/CD-2, FAH-rGO/CD-3 and FAH-rGO/CD-4.

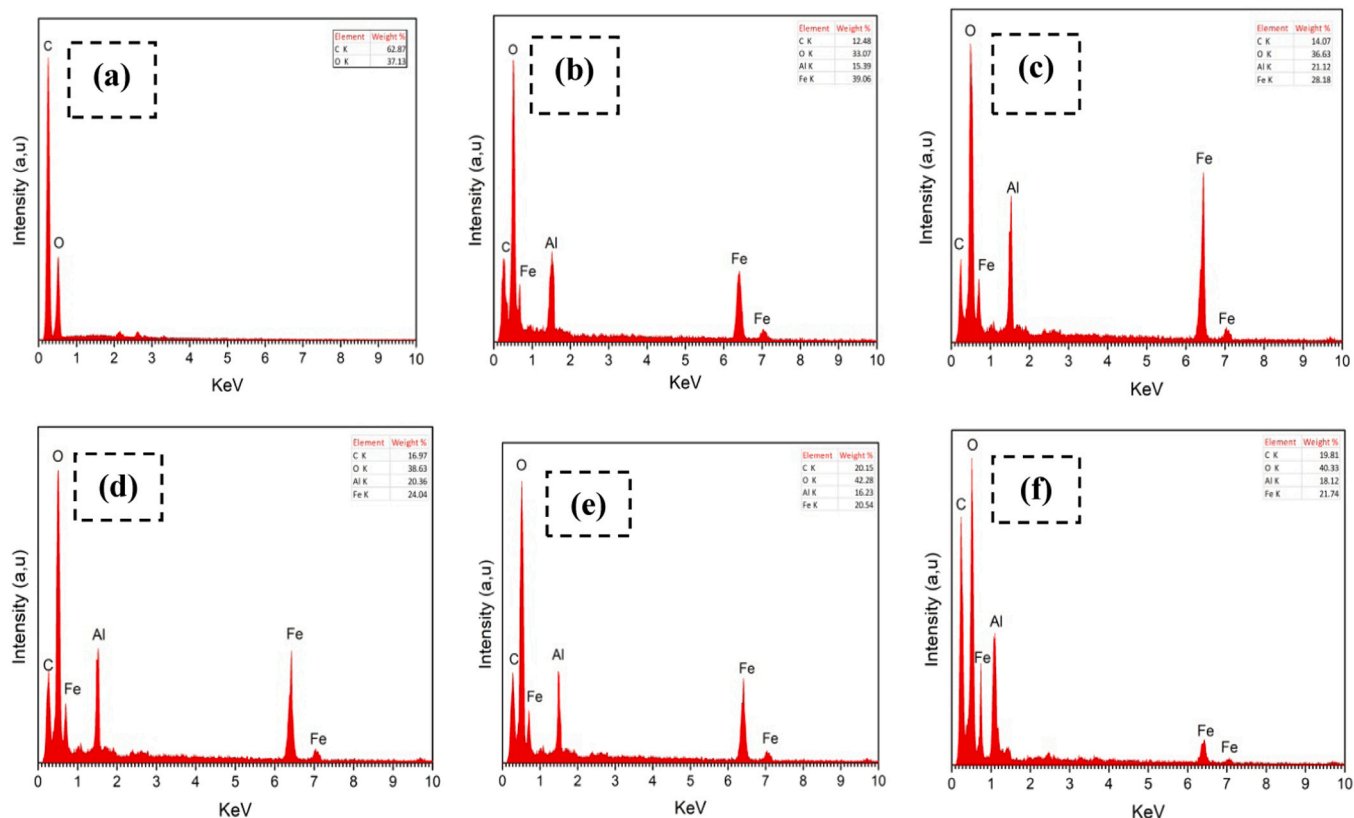


Fig. 3. (a-f) EDS spectrum of GO, FAH-rGO, FAH-rGO/CD-1, FAH-rGO/CD-2, FAH-rGO/CD-3 and FAH-rGO/CD-4.

reported in our previous studies [4,16]. Briefly, 0.2 g of GO was ultrasonicated in 100 ml of DI water for one hour to yield well dispersed GO solution. Then, 4 g of $\text{FeCl}_2 \cdot 0.4 \text{H}_2\text{O}$ and 2.4 g $\text{AlCl}_3 \cdot 0.6 \text{H}_2\text{O}$ was mixed in GO solution with continued stirring for 1 h up to pH attained at 10 ± 0.5 by adding 4 mol/L of NaOH solution. Then, the colloidal solution was transferred to 100 ml of stainless-Teflon lined autoclave heated at 110°C for 24 h. The resultant products were washed and centrifuged with DI water and ethanol. The final product was dried at 70°C under vacuum. Pure FAH was synthesized by using above method without GO.

2.3. Synthesis of FAH-rGO/CD

At the beginning, 0.5 wt% of FAH-rGO was ultrasonically dispersed for 1 h in DI water to attain a brown solution. Simultaneously, 0.5 wt% of β -CD was dissolved in 100 ml of DI water under stirring for several minutes. Then, FAH-rGO homogeneous solution was added as dropwise to the β -CD solution under stirring for 24 h. The desired products were rinsed and centrifuged using DI water and ethanol, respectively. Finally, the residual was dried in vacuum at 50°C . The different weight percentages of β -CD (0.5 wt%, 1 wt%, 1.5 wt% and 2 wt%) in FAH-rGO nanocomposites were prepared by using the same method and are denoted as FAH-rGO/CD-1, FAH-rGO/CD-2, FAH-rGO/CD-3 and FAH-rGO/CD-4 respectively, for further analysis [55].

2.4. Characterization techniques

Diffraction patterns of the synthesized samples were performed by using X-Ray diffractometer (Shimadzu XRD – 6000) with $\text{Cu K}\alpha$ radiation operating at 40 kV and 30 mV. Structural morphology of the nanocomposites was examined by Field Emission Scanning Electron Microscope (SIGMA HV-CARL ZEISS) and High Resolution Transmission Electron Microscope (JEOL-JEM-2010) acquired at an accelerating voltage of 200 kV with SAED pattern. The elemental compositions of

samples were investigated with Energy Dispersive Spectroscopy (EVO, CARL ZEISS). The N_2 adsorption-desorption analysis (ASAP-2020 V3H) was used to analyze the surface area, pore radius and pore volumes of the samples. Fourier Transform Infrared spectra of functional groups in composites were recorded (Bruker Alpha FTIR spectrometer) by using the KBr pellets technique.

2.5. Adsorption experiments

Equilibrium batch techniques were accomplished to analysis the different parameters of adsorption such as the effect of pH, effect of contact time and effect of adsorbent dosages. In general, the adsorption experiments were carried out in polyethylene tubes containing different amount of adsorbent dispersed thoroughly in 100 ml of As (V) solution of concentration (100 mg/L). The tubes were then placed in the mechanical shaker rotating at 150 rpm at 30°C for 24 h. After complete equilibrium adsorption, the adsorbent was collected through strong permanent magnet and the supernatant was taken for the quantitative analysis to determine the remaining concentration of As (V) ions using UV-Vis double beam spectrometer (AU-2701) [56,57]. The adsorption capacity (q_e) of synthesized adsorbent was calculated by the Eq. (1),

$$q_e = \frac{(c_0 - c_e) * v}{m} \quad (1)$$

Where, c_e and c_0 are the equilibrium and initial concentration of As (V) (mg L^{-1}), v and m are denoted as the volume of the solution (L) and mass dosage of adsorbent (g). Desorption experiments were conducted to investigate the regeneration of spending adsorbent using 0.1 M of NaOH as eluting agents under ultrasonic agitation. After desorption, the solution was filtered and its residual was dried at 60°C under vacuum, and then reused for the arsenate adsorption under the same condition. All reported data of the batch experiments were determined to be the average value of the triplicate determinations.

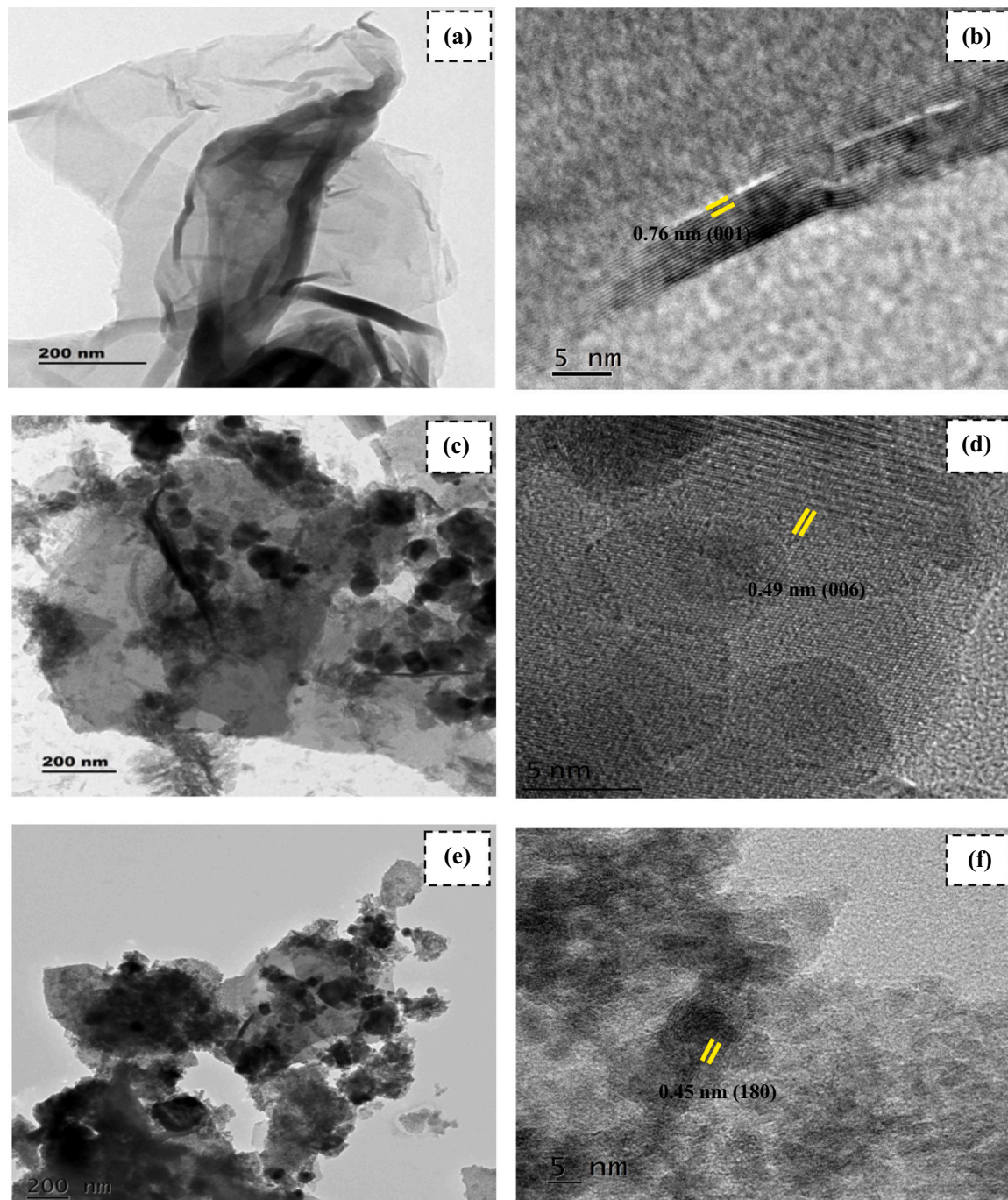


Fig. 4. (a-b) HRTEM images of GO at high and low magnification; (c-d) HRTEM images of FAH-rGO at high and low magnification; (e-f) HRTEM images of FAH-rGO/CD-4 at high and low magnification.

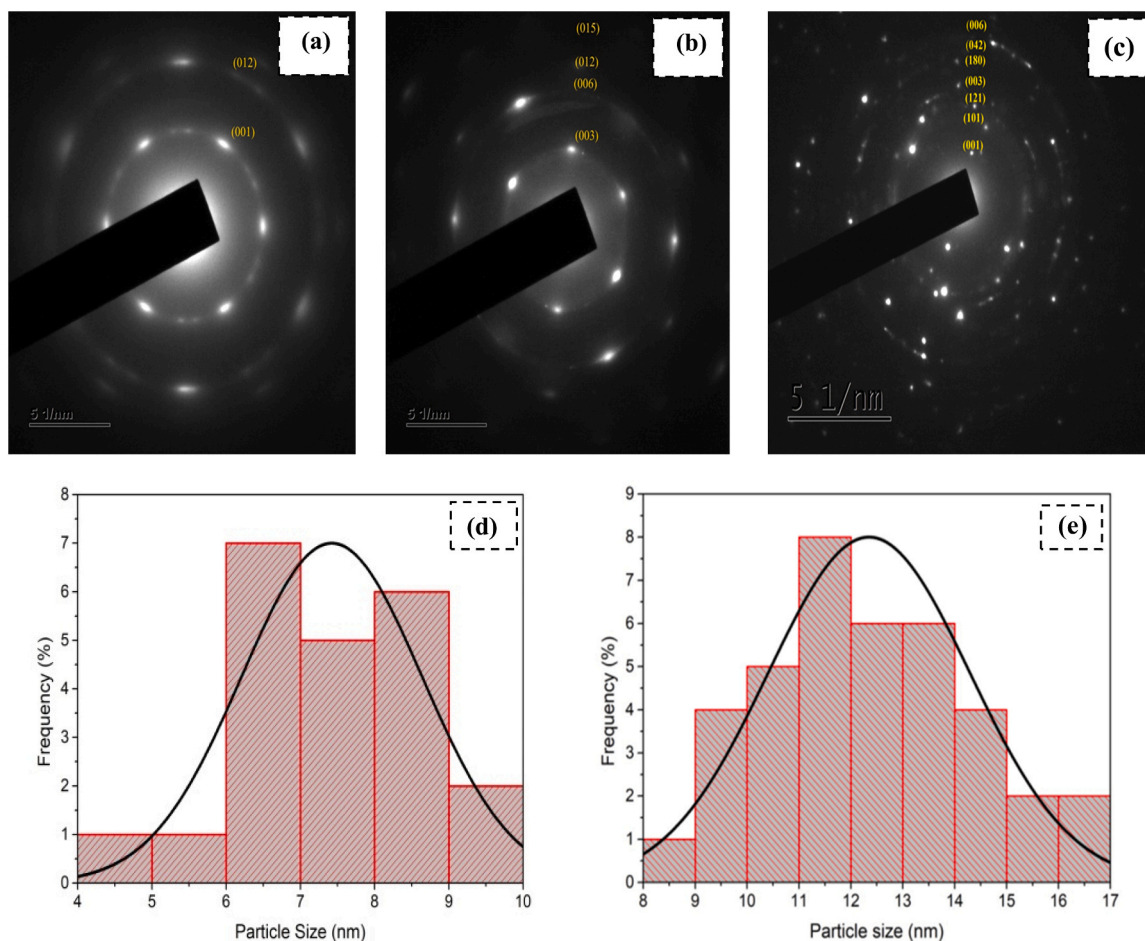


Fig. 5. (a-c) SAED patterns of GO, FAH-rGO & FAH-rGO/CD-4, (d-e) Particle size distribution of FAH-rGO, FAH-rGO/CD-4.

3. Results and discussion

3.1. Characterization of FAH-rGO/CD composites

XRD diffraction patterns of prepared composites of graphite, GO, FAH-rGO and FAH-rGO/CD (1–4) are shown in Fig. 1(a–b). After oxidation, the typical characteristic peaks of graphite ($2\theta = 25.19^\circ$, $d_{001} = 0.35$ nm) get disappear and are replaced by well-defined peaks ($2\theta = 9.36^\circ$, $d_{001} = 0.94$ nm) within an increase of 0.59 nm in the interlayer space to strengthen the atomic-roughness on the graphite layer. In Fig. 1 (a), XRD patterns of LDH show their characteristic basal peaks at 11.77° and 23.33° values corresponding to (003) and (006) planes respectively, while the peak position at 34.92° and 40.08° with miller indices (012) and (015) represent non basal peaks respectively, which are in good agreement with reported literature [57–59]. After intercalation of β -CD in FAH, the typical basal plane ($d_{003} = 0.76$ nm) of FAH shifts to lower angle at $2\theta = 7.73^\circ$ ($d_{003} = 1.14$ nm), with significant increase of 0.38 nm in the d -spacing. The enlargement of interlayer distance in FAH-rGO/CD is mainly attributed to ion-exchange mechanism between the FAH-rGO and FAH-rGO/CD ions [53]. The gallery height of the FAH-rGO/CD-4 is calculated as 0.66 nm through the d -spacing of FAH-rGO/CD-4 substrate from the laminate thickness of LDH (0.48 nm) [60]. It may be concluded that, the β -CD molecules had been intercalated as the monolayer arrangement into the gallery with their cavity axes perpendicular in the FAH-rGO layer [32]. The lattice constant parameters of FAH-rGO and FAH-rGO/CD-4 are calculated as $a = 0.31$ nm; $c = 1.90$ nm and $a = 0.31$ nm; $c = 2.20$ nm, respectively. Moreover, the lattice parameter “a” is almost constant for pure and composite samples than c. Hence, there is no change in the average distance between the

metal ions and $\text{Fe}^{2+}/\text{Al}^{3+}$ ratio after the intercalation of β -CD. There is no significant shift in reflection line diffraction peaks at (012) and (015), which indicate the intercalation of β -CD with FAH-rGO has not modified the layer structure instead of lattice spacing [57].

The structural morphology of the prepared nanocomposites was investigated by the FESEM analysis. In Fig. 2(a), GO was exfoliated as sheet like structure with smooth and corrugated edge surface. While intercalation process, the FAH layered double hydroxide was deposited on the GO surface as hexagon flake like structure with uniformity through homogeneous and the slow nucleation process, which is shown in Fig. 2(b) [4,61]. The corresponding thickness of LDH is ≈ 2.78 nm and their outer layer promotes the exfoliation rate for better binding of polymers [16,58,62]. Fig. 2(c–f) exhibits the CD particles embedded in the surface of the LDH. When CD wt% increases as 2%, the CD particles were deposited on the entire LDH surface, including internal, external and surface walls to enhance the rate of adsorption of LDH as shown in Fig. 2(f) [63]. In Fig. 3(a–f), the EDS spectrum reveals the chemical purity of the prepared samples and confirms the presence of elemental compounds such as carbon, oxygen, iron and aluminum in GO, FAH-rGO, FAH-rGO/CD (1–4) [64].

The HRTEM images of GO, FAH-rGO and FAH-rGO/CD-4 and their SEAD patterns are illustrated in Fig. 4 & 5. The Fig. 4(a) demonstrates the layer like morphology of GO, which were wrinkled and scrolled into the sheet like structure that indicate the exfoliation of GO [4,55]. After the intercalation of FAH in GO, the hexagonal shaped double layered hydroxide nanoplates (FAH) are completely interacted on the layer surface of GO [31]. The intercalated FAH produced some wrinkles on layer to prevent the aggregation nature of GO surface which is clearly denoted in Fig. 4(c) [4,35]. After the combination of β -CD with FAH-rGO

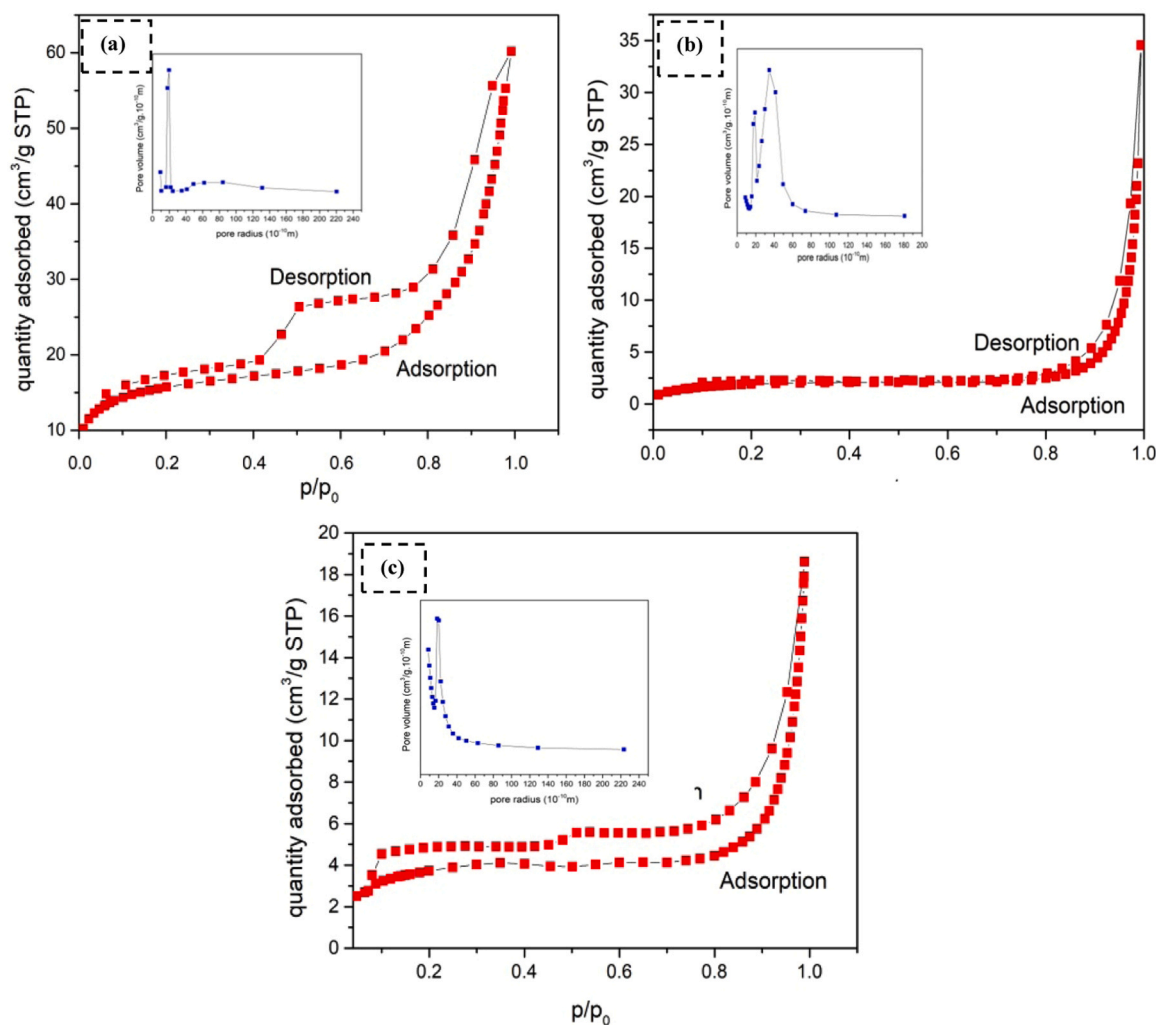


Fig. 6. (a-c) N_2 adsorption-desorption isotherms of GO, FAH-rGO, FAH-rGO/CD-4.

Table 1

Surface area, pore volume and radius of synthesized adsorbents.

Adsorbents	Surface area ($m^2 g^{-1}$)	Pore volume ($cm^3 g^{-1}$)	Pore radius (nm)
FAH-rGO	50.0451	0.0930	4.1044
FAH-rGO/CD-1	98.2974	0.1569	3.4578
FAH-rGO/CD-4	145.3542	0.2876	2.0457

to form FAH-rGO/CD composites, many small β -cyclodextrin have been accumulated on the surface of FAH-rGO. The diameter calculated from histogram images is ≈ 6 – 8 nm for FAH-rGO and FAH-rGO/CD composites is 11 – 14 nm and are represented in Fig. 5(d,e). The Fig. 4(b,d&f) shows the lattice fringes with d -spacing as ≈ 0.79 , 0.49 and 0.47 nm, which clearly reflects the (001), (006) and (180) planes of GO, FAH-rGO and FAH-rGO/CD-4 respectively [4].

The properties of surface area and porosity of prepared nanocomposites were investigated to employ the N_2 adsorption-desorption analysis and are denoted in Fig. 6. In the hydrothermal synthesis of FAH-rGO, the GO nanosheets get separated by FAH-moieties to provoke the surface area through intercalation [4,16]. While in the polymerization process of CD nanocomposites, the β -cyclodextrin has been assembled on the surface of FAH-rGO to increase their surface area [55–66]. The Barrett-Joyner-Halenda (BJH) method was followed to

determine the pore radius and volume of prepared composites. When the FAH moieties started their intercalation with CD moieties in GO matrix, the trend of the pore radius started decreasing. The obtained N_2 adsorption-desorption isotherms is classified as a type IV hysteresis loop through the pressure value as $p/p_0 = 1$, which denotes the presence of mesoporous and less agglomerated materials in nanocomposites [31]. From results, the high surface area and more active sites of FAH-rGO/CD-4 nanocomposite in comparison with the other two composites which led to the conclusion that FAH-rGO/CD-4 could be used as a good candidate for water treatment. Table 1 summarizes the measurement value of surface area, pore radius and pore volume of as-synthesized samples.

The FTIR pattern of GO, FAH-rGO and FAH-rGO/CD-4 nanocomposites is shown in the Fig. 7. From Fig. 7(a), the bands obtained at 3472 cm^{-1} and 3549 cm^{-1} assigned as the stretching vibration of interlayer water molecules of hydroxyl groups in both GO and FAH surface. The peaks at 2351 cm^{-1} and 1790 cm^{-1} can be declared as the C-H and C=O stretching vibration and the predominant peaks of graphitic vibration is observed at 1609 cm^{-1} . The stretching modes of the C-OH, C-O-C and C-O group bands are observed at 1415 cm^{-1} , 1222 cm^{-1} and 1061 cm^{-1} respectively. The weak peaks around 842 cm^{-1} and 595 cm^{-1} are represented as the epoxy groups of GO [4,36,53]. In Fig. 7(b), the characteristic peaks assigned with C-O and C=O get disappeared and confirms the reduction of oxygen groups in GO, to form rGO. The peaks 2369 cm^{-1} and 1383 cm^{-1} can be related to the water and hydrogen bonding between the layered double hydroxide.

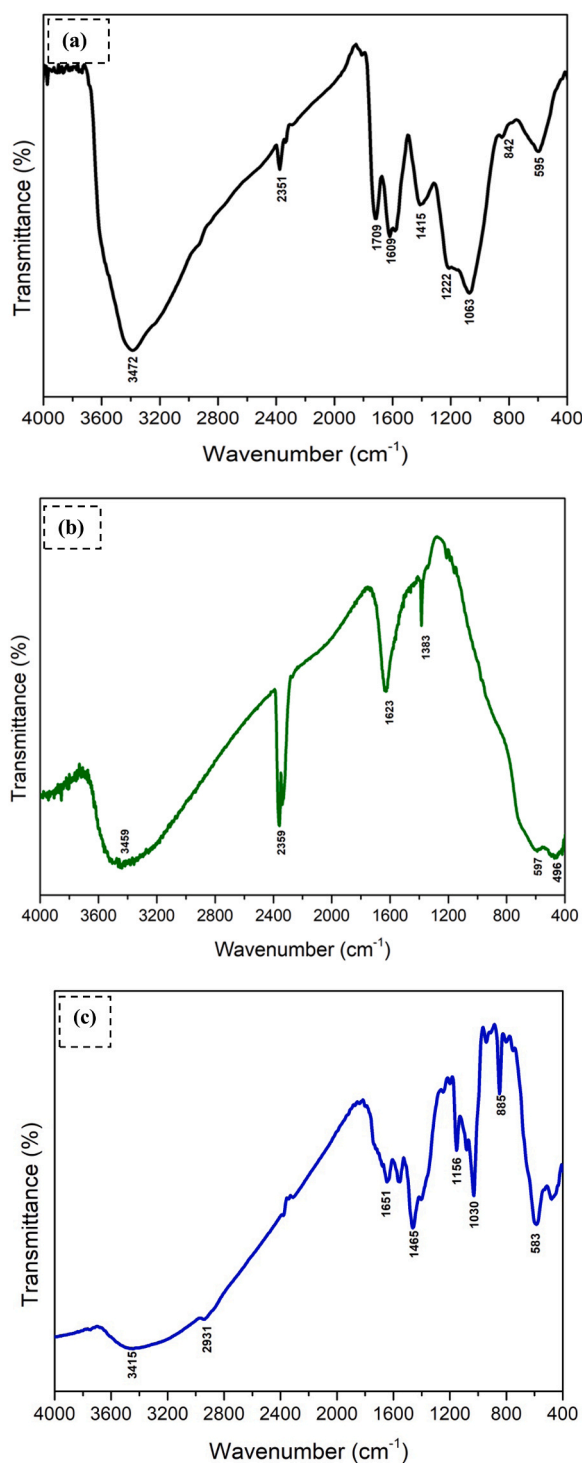


Fig. 7. (a-c) FTIR images of GO, FAH-rGO and FAH-rGO/CD-4.

The broadening and shifting of hydroxyl groups in FAH towards lower wavelength indicates the strong interaction of GO and FAH. The bonding of FAH and GO is reflected from the strong stretching vibration of C=O at 1623 cm^{-1} . All other peaks below 800 cm^{-1} indicates the lattice vibration of LDH as M-O, M-O-M and M-O-M respectively [49,67,68]. From Fig. 7(c), the strong interaction of hydroxyl groups in β -CD and FAH-rGO are represented at 3415 cm^{-1} and the primary peaks of β -CD assigned in 2971 and 885 cm^{-1} as $-\text{CH}_2$ stretching vibration and R-1, 4-bond skeleton vibration of β -CD. The peaks around 1165 cm^{-1} and 1030 cm^{-1} as assigned to the asymmetric glucose vibration of β -CD. The

peaks around $1650\text{--}1465\text{ cm}^{-1}$ denotes the C-H and C-N stretching vibration of prepared composites. The metal-oxygen containing modes of FAH-rGO/CD-4 are observed below at 800 cm^{-1} [53,54].

3.2. Effect of contact time

Effect of contact time on synthesized adsorbents for As (V) adsorption were investigated by conducting the adsorption experiments at different time periods of 60–600 min at fixed pH 7 at room temperature. From Fig. 8(a), the efficiency of As (V) removal of all the adsorbents increased with contact time, to conclude higher removal efficiency of adsorbent. The rate of adsorption was in a fast manner from 60 min up to 360 min and reached maximum adsorption due to availability of a large number of active sites which adsorb As (V) anions. Compared to other materials, the FAH-rGO/CD-4 shows the high removal efficiency of As (V) ions. The presences of unique hydrophobic cavity of CD with high wt % in composites have significantly improved the selective adsorption of As (V) anions. Equilibrium of adsorption starts to attain at above 360 min as the adsorbent reaches its saturation condition of their active sites. Hereby, FAH-rGO/CD-4 composite shows the highest removal efficiency of adsorption As (V) ions than FAH-rGO/CD-1 and FAH-rGO which leads to the further adsorption analysis [57].

3.3. Effect of adsorbent dosage

Different weight dosages of adsorbent were tested to analysis the optimum weight dosage of FAH-rGO/CD-4 in the range of 0.01–0.07 g/L which is shown in Fig. 8(b). It can be noted that the As (V) removal efficiency of the adsorbent increased with weight dosage in the presence of a large number of activated sites in the surfaces. The adsorption rate of FAH-rGO/CD-4 starts to reach a maximum at 0.07 g/l and above this dosage the adsorbent does not show any significant change in removal capacity of adsorbent. Therefore 0.07 g/l dosages of adsorbent were taken into account as the mass dosage for further kinetic studies [57].

3.4. Effect of pH

Generally, the pH of the adsorbent can affect the sorption of metal ions in aqueous medium due to presence of H^+ ions. The effect of pH experiments was executed in the range of pH 2–11 by using 0.1 M HCl/NaOH solution at constant contact time, the mass of adsorbent and adsorbate concentration at room temperature and the results are exhibited in Fig. 8(c). The removal efficiency of FAH-rGO/CD-4 was reached maximum (98.4%) at $\text{pH} \leq 7$ and gets remarkably decreased to minimum (17.28%) at $\text{pH} \geq 8$. The predominant species of As (V) can occur in the aqueous solution as the forms of H_2AsO_4 , HASO_4^{2-} and AsO_4^{3-} in the pH ranging from pH 2–11 [53]. At the acidic condition, the positive charges in adsorbent might carry positive charges such as the $-\text{OH}_2^+$, $-\text{COOH}^+$ groups, gets hydrogenated as $-\text{COOH}_2^+$, $-\text{OH}_2^+$, that enhances the capture of negative ionic form of As (V) anions through electrostatic attraction. At high pH condition, there is no interaction between the negative charge of adsorbent and adsorbate because of the dehydrogenation of surface $-\text{OH}$ and $-\text{COOH}$ groups of the adsorbent in the presence of more number of H^+ ions. Thereby, the electrostatic repulsion force between the negative charge of adsorbent and adsorbate induces the less capture of anionic As (V) molecules. Hence, the high removal efficiency for As (V) anions on FAH-rGO/CD-4 is due to the electrostatic interactions between their surface charges [53,67].

3.5. Adsorption isotherms

Adsorption isotherm studies were utilized to examine the mechanisms of adsorption and interaction between the liquid-solid phases, which helps in designing the desired adsorption system. The equilibrium adsorption studies were accomplished by using two adsorption isotherms, Langmuir and Freundlich models. Langmuir model is commonly

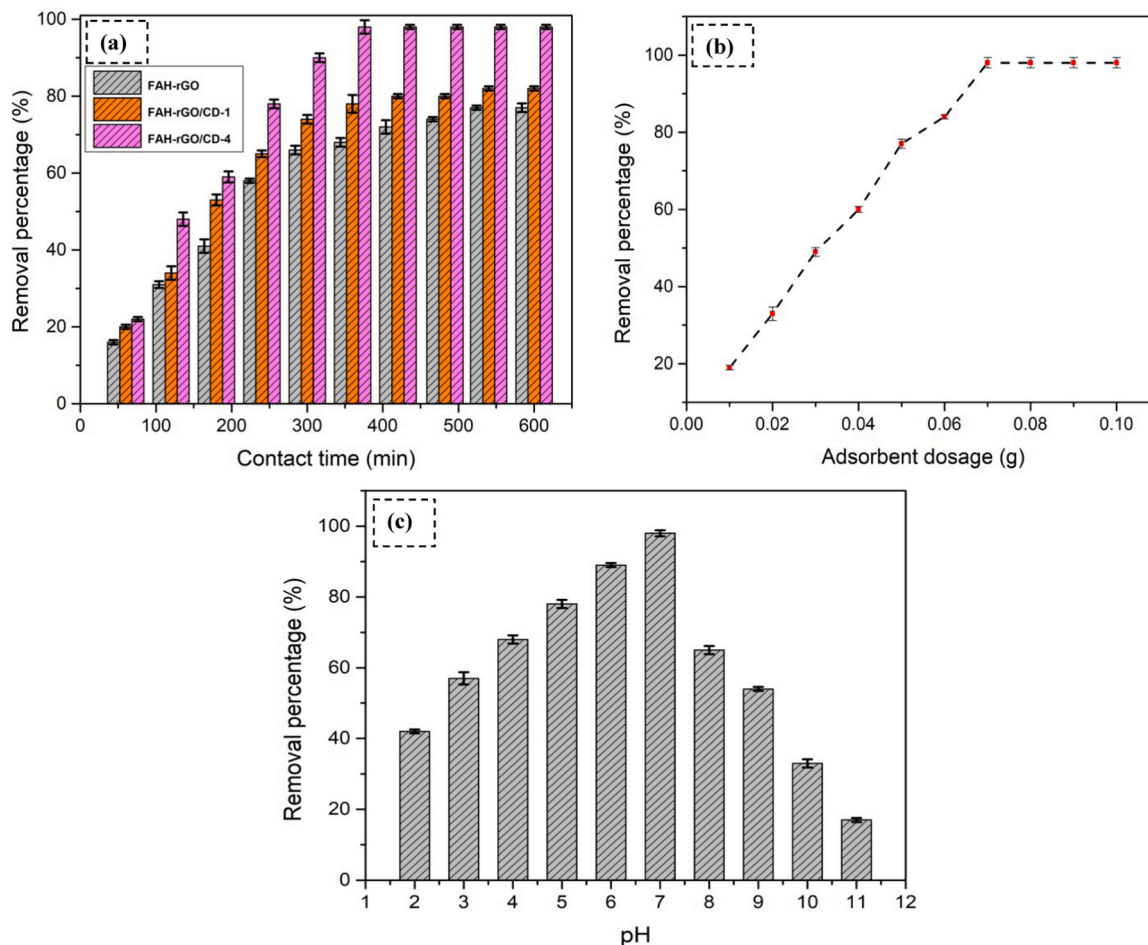


Fig. 8. (a-c) Effect of contact time, effect of adsorbent dosage and effect of pH of adsorbents on As (V) removal.

used to interpret the monolayer adsorption on the homogeneous surface [21,69]. The mathematical form of Langmuir model is expressed in the Eq. (2).

$$\frac{c_e}{q_e} = \frac{1}{(q_{max} * b)} + \frac{c_e}{q_{max}} \quad (2)$$

Where q_{max} is the maximum adsorption capacity and b is the binding constant related to the energy of adsorbent and their values calculated from the relevant slope and intercept values of linear plot c_e and c_e/q_e are shown in Fig. 9(b). The dimensionless separation factor R_L of Langmuir model expressed in Eq. (2) is given by,

$$R_L = \frac{1}{1 + bC_0} \quad (3)$$

In Table 2, the calculated R_L values lie between the range of 0–1 and hence confirms the favorable adsorption of As (V) by FAH-rGO/CD [70]. Freundlich model is defined as multilayer adsorption on heterogeneous surface [20,21]. The mathematical expression of Freundlich isotherms is represented in Eq. (4).

$$\log q_e = \log k_f + \frac{1}{n} \log c_e \quad (4)$$

Where, n and K_f values are related to the adsorption intensity and capacity of adsorbent respectively, and it can be calculated from the slope and intercept values of the linear plot of $\log c_e$ Vs $\log q_e$ as shown in Fig. 9(c). The obtained value of $1/n$ is in the range of 0.1–0.5. It reflects that the As (V) anions can be easily adsorbed by the FAH-rGO/CD surface [35,71]. To evaluate the suitable method among the two different

models, it is needed to process the linear least square method which gives the adequacy of isotherm models with best equilibrium data [8,9].

The data of adsorption isotherms on As (V) anions were determined to be a better fit to the Langmuir model with the high correlation coefficient R^2 value (0.9899) than the low R^2 value (0.8329) of Freundlich model. This denotes that the adsorption has occurred by monolayer coverage and summarized in Table 2. This may be attributed by the hydroxyl groups of FAH-rGO and β -cyclodextrin on the outer layer of graphene oxide [56].

3.6. Adsorption kinetics

Adsorption kinetics were employed to establish the interaction of adsorption and transport mode of adsorption through pseudo first and pseudo second order model to quantify the changes of adsorption by means of time [25]. The mathematical expression of the pseudo first order and pseudo second order are represented by the following Eqs. (5) and (6).

$$\log(q_e - q_t) = \log q_e - \frac{k_1 t}{2.303} \quad (1)$$

$$\frac{t}{q_t} = \frac{1}{k_2 q_e^2} + \frac{t}{q_e} \quad (6)$$

Where, q_e and q_t denotes the adsorbed amount (mg g^{-1}) at equilibrium and at time t respectively. k_1 and k_2 are the pseudo first and second order models [35]. The slope and intercept values in the plot of t Vs $\log(q_e - q_t)$ and t Vs t/q_t were given by the values of q_e and k which is shown in Fig. 10 (b-c). The various parameter values of pseudo first and second

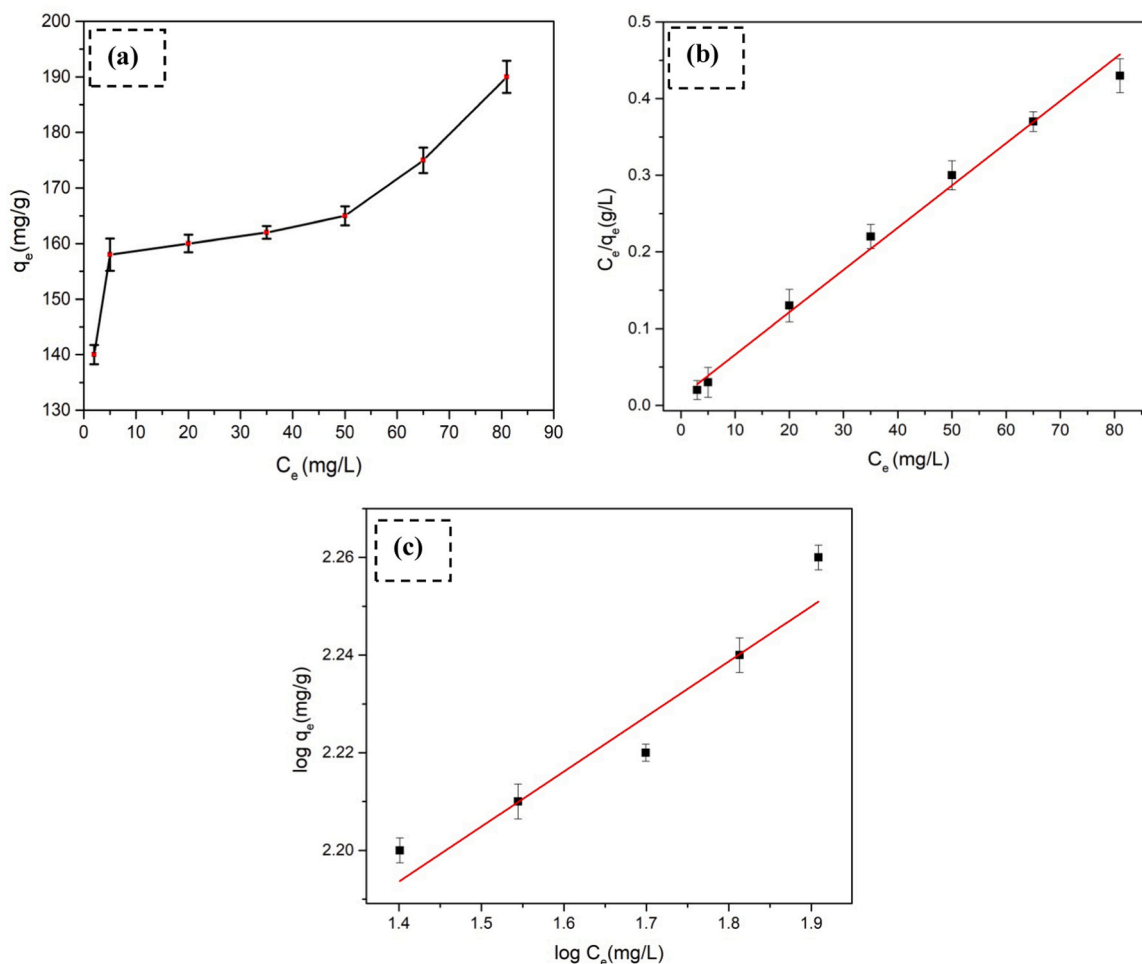


Fig. 9. (a) Equilibrium isotherms of As (V) on FAH-rGO/CD-4, (b-c) Langmuir and Freundlich isotherms for As (V) on FAH-rGO/CD-4.

Table 2

Adsorption isotherms of FAH-rGO/CD-4 on As (V) removal.

Langmuir isotherm model				Freundlich isotherm model			
q_{max} ($mg\ g^{-1}$)	R_L	b ($L\ mg^{-1}$)	R^2	$1/n$	n	k_f ($(mg/g)\ (L/mg)^{1/n}$)	R^2
185.52	0.9651	0.3610	0.9899	0.0941	10.6214	7.92712	0.8329

order are listed in Table 3. The obtained values of the equilibrium adsorption capacity of pseudo second order models were much closer to the experimental data of adsorption. Thus, it can be concluded that, the pseudo second order model was predominant and the adsorption attained with the help of rate-limiting steps involves valance forces throughout the exchanging and sharing of electrons between the adsorbent and adsorbate [30].

3.7. Effect of co-existing substances

Natural groundwater usually contains some of the coexisting substances such as chloride, sulfate, nitrate, phosphate and bicarbonate ions, which can compete the adsorption and could affect the As (V) adsorption. To study the influences of these coexisting anions on sorption of As (V), the above anions were added to adsorbate solutions at different concentrations, and As (V) removal property was studied. The Fig. 11(a) illustrates the effect of coexisting ions on adsorption of As (V). The results suggested that, the removal efficiency of As (V) ions was decreased in the presence of inference anions in the order of, phosphate>bicarbonate>sulfate>chloride>nitrate. These inferences of anions

on adsorption of As (V) may be due to their relative interactions with the adsorbent. The results suggested that, the phosphate and bicarbonate anions have high influences on the adsorption rate of As (V) on comparison with other than anions, which may be due to adsorption of the multivalent anions than monovalent anions [72–74]. Thus, the as-synthesized FAH-rGO/CD composite might be effectively utilized to remove As (V) ions in aqueous solution containing the highest concentration of sulfate, nitrate and chloride anions.

3.8. Regeneration of saturated adsorbents

The investigation of recycling and regeneration ability on the adsorbent is imperative for its commercial application in wastewater treatment. After adsorption, the As (V) adsorbed FAH-rGO/CD nanocomposite was easily collected in a fast manner because of its magnetic properties which is shown in Fig. 11(c). To investigate the effect of adsorption-desorption, As (V) adsorbed FAH-rGO/CD nanocomposite was treated with NaOH and the results of five consecutive adsorption-desorption are shown in Fig. 11(b). The efficiency was found to be 96%, for the first cycle and starts to decrease up to 89% for future four

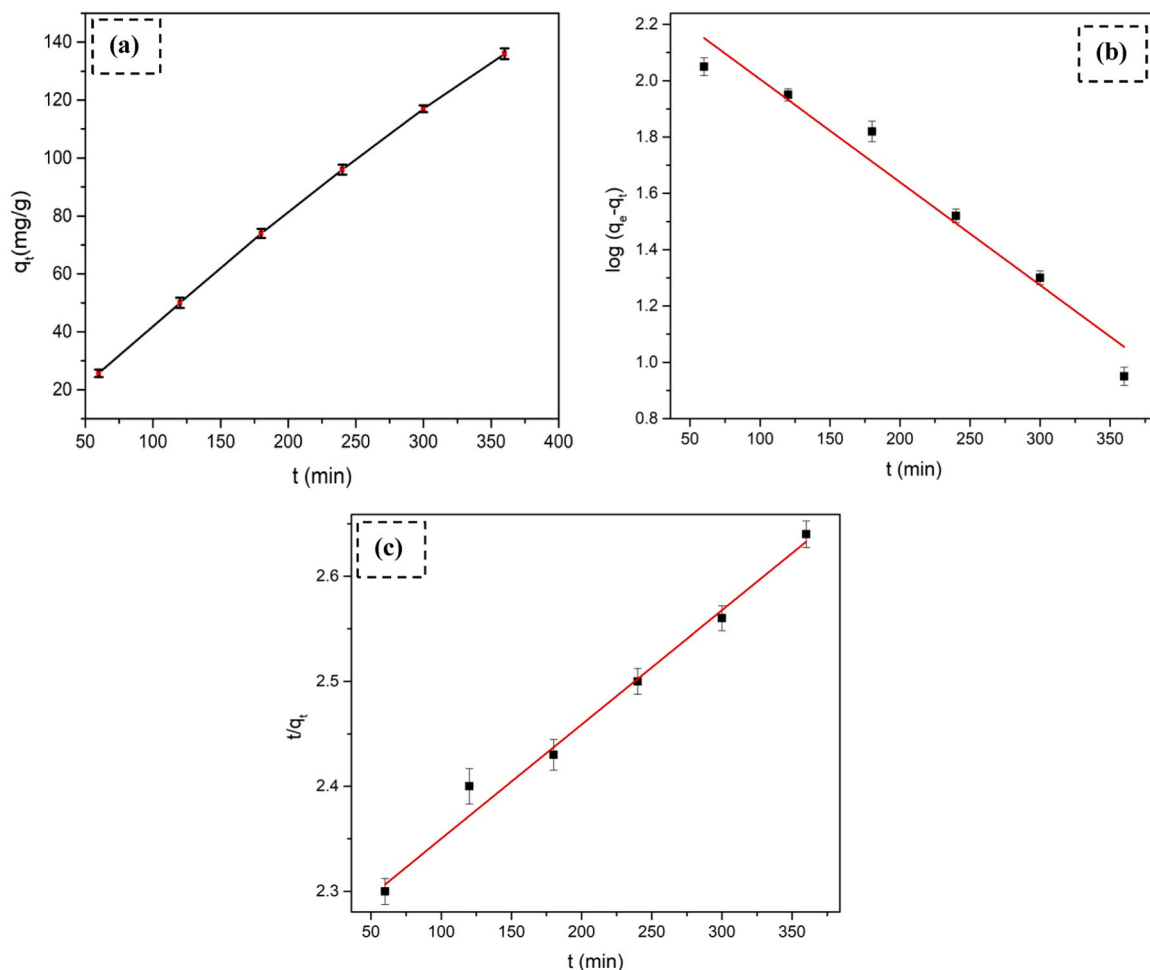


Fig. 10. (a) Time profile of FAH-rGO/CD-4 on As (V) removal, (b-c) Pseudo first and Pseudo second order Kinetics for As (V) removal on FAH-rGO/CD-4.

cycles. During regeneration, the As (V) adsorbed FAH-rGO/CD composite cannot desorb the As (V) anions completely from the cavity of cyclodextrin and also active sites of hydroxyl groups decreases in adsorption, causing slight decrease in As (V) anions adsorbed by FAH-rGO/CD [30]. Hereby, the prepared adsorbents can be recycled and reused for wastewater treatment.

3.9. Characterization analysis for As (V) adsorbed FAH-rGO/CD

The variations in morphology, elemental compositions and functional groups of As (V) adsorbed FAH-rGO/CD-4 nanocomposites were required to study the election of suitable good adsorbent. Before and after SEM images of As (V) adsorbed FAH-rGO/CD is exposed in Fig. 12 (a,b) and it indicates that the sheet structure of adsorbent gets distorted

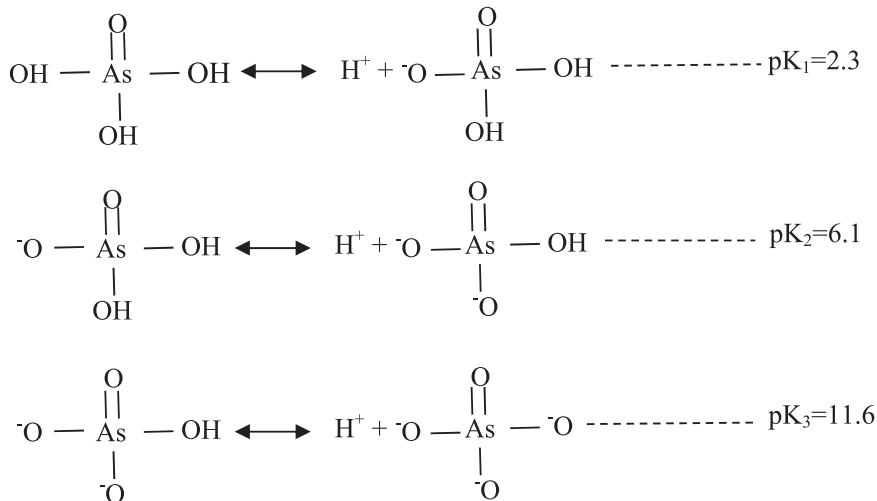
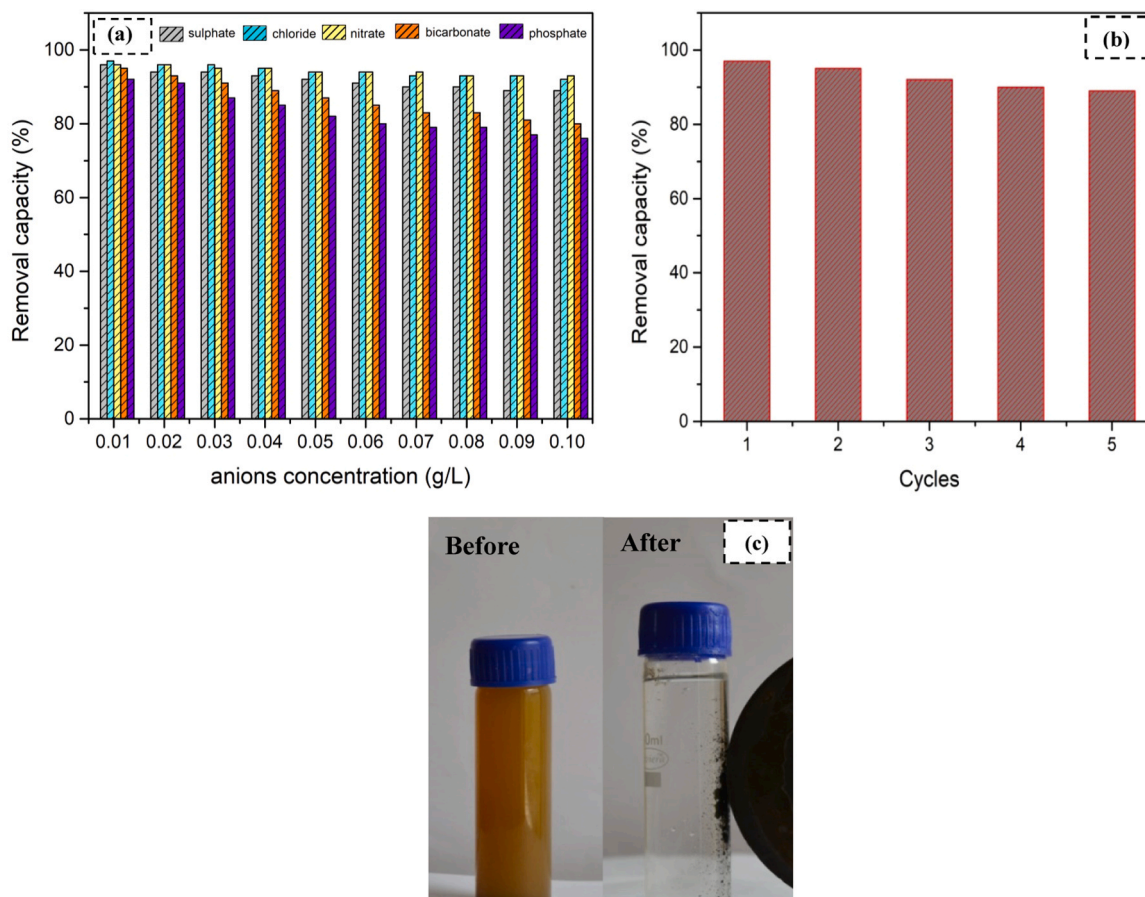


Table 3

Adsorption kinetics of FAH-rGO/CD-4 on As (V) removal.

Pseudo first order kinetic model				Pseudo second order kinetic model		
q_{exp} ($mg\ g^{-1}$)	q_{cal} ($mg\ g^{-1}$)	k_1 (min^{-1})	R^2	q_{cal} ($mg\ g^{-1}$)	k_2 ($g\ mg^{-1}\ min^{-1}$)	R^2
140.10	12.06	0.1008	0.8091	146.60	2.6647×10^{-5}	0.9836

**Fig. 11.** (a) Effect of coexisting anions on As (V) adsorption; (b-c) Desorption analysis and separation process of FAH-rGO/CD-4.

and produces a number of smaller particles on their surface which represents the sorption of As (V). The morphological changes accomplishes that the Fe^{2+} and Al^{3+} ions were discharged from the layered structure to form another phase of adsorption [30,75]. The immediate evidence of the As (V) adsorption was depicted by EDS spectrum, which is shown in Fig. 12 (c). The weight percentages of oxygen were reduced after adsorption due to the ionic interaction between the adsorbate and adsorbent. The ionic interaction of -OH on As (V) anions were confirmed by the broadening and shifting of intensity towards lower wavelength at $3278\ cm^{-1}$. The As-O-M bending vibration peak at $842\ cm^{-1}$ established the adsorption of As (V) anions in FAH-rGO/CD-4 surface [30,72]. The typical peaks of the β -CD on As (V) adsorbed FAH-rGO/CD-4 were confirmed by their peaks at $1665\ cm^{-1}$, $1460\ cm^{-1}$ and $1154\ cm^{-1}$ and which is observed in Fig. 12(d). Thus, as-prepared adsorbent can be used in As (V) removal.

4. Removal mechanism

Novel nanoadsorbent FAH-rGO/CD was effectively developed by the simple chemical route method. At the beginning, modified Hummer's

method was followed to prepare GO and the FAH moieties was intercalated between the GO through hydrothermal method via ionic interaction of negatively charged -COOH and -OH groups of GO and/or by electrostatic interactions of π - π electrons in the aromatic rings of GO with the positively charged LDH [38]. And then, the CD moieties were deposited on the external layer of FAH-rGO with strong interactions hydroxyl (-OH) groups of CD with oxygen functional groups in GO and positively charged LDH through ex-situ polymerization process to construct a host-guest inclusion complexes [57]. Generally, the surface of graphene oxide contains the various oxygen-containing groups, including hydroxyl, carboxyl, and epoxy groups which promote the rate of adsorption to bind metal ions. One of the specific significant features of cyclodextrin is its facility to combine selected various metal ions to form stable host-guest inclusion through their cavities [57]. Metal hydroxide in layered double hydroxide influences their boundary layer to capture the heavy metal ions [16]. In adsorption process, As (V) ions identified as the primary species such as $H_2AsO_4^-$, $HAsO_4^{2-}$ and AsO_4^{3-} on an aqueous solution at the pH ranging from pH 2–12 and their acid dissociation equilibrium reactions were represented given below [34]

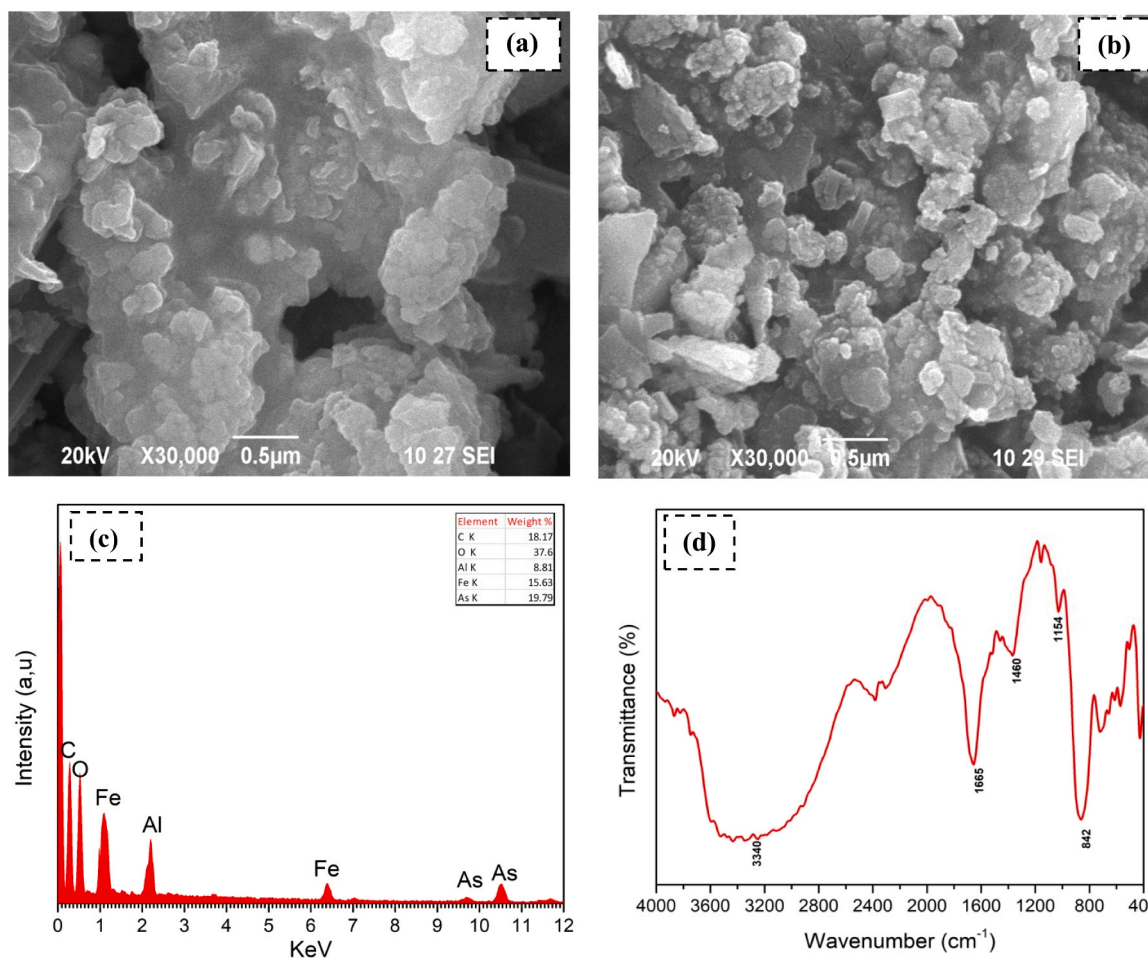


Fig. 12. (a,b) SEM images of FAH-rGO/CD-4 before and after adsorption of As (V), (c-d) EDS spectrum and FTIR images of FAH-rGO/CD-4 after adsorption of As (V).

Due to strong protonation occurred at $\text{pH} \leq 7$, the oxygen functional groups on the surface of FAH-rGO/CD was converted as positively charged groups such as $-\text{COOH}_2^+$ and $-\text{OH}_2^+$ through the presence of more number of H^+ ions [76]. Therefore, the positively charged functional groups of FAH-rGO/CD nanocomposites react with the negatively charged As (V) ions through electrostatic attraction at acidic pH [53]. As it can be observed that, higher adsorption of As (V) at acidic pH condition may be caused by electrostatic attraction of the cationic surface of adsorbent sites and the anionic adsorbate ions and its interactions were shown in Fig. 13 (a). Thus, as-synthesized FAH-rGO/CD nanoadsorbent has the exquisite adsorption capacity benefiting from hydrophobicity of β -cyclodextrin, large surface area and boundary hydroxyl groups in surface of GO and LDH. The schematic illustration was as shown in Fig. 13 (b).

4.1. Comparison of the adsorption behavior of FAH-rGO/CD based on other adsorbents

The adsorption behavior of FAH-rGO/CD towards As (V) adsorption was evaluated with respect to its adsorption capacity of other LDH/GO/ β -CD derived adsorbents, which is summarized in Table 4. Compared with some adsorbents, the adsorption capacity of as-synthesized adsorbent is higher, indicating that the high wt% of CD in FAH-rGO composite improves the removal of As (V) ions.

5. Conclusion

In summary, the magnetically separable FAH-rGO/CD nanocomposites were synthesized with high active surface area through simple chemical route method and the formation of composite were investigated by various analytical studies, including XRD, FESEM, EDS, HRTEM and FTIR. N_2 adsorption-desorption analysis revealed that, the as-prepared FAH-rGO/CD-4 composite had a high surface area ($145.35 \text{ m}^2 \text{ g}^{-1}$) through the intercalation of β -CD molecules on the surface of FAH-rGO composite. It is noteworthy that the FAH-rGO/CD-4 has excellent removal efficiency (98%) for the As (V) adsorption owing to the high surface area of GO, hydrophobicity of β -cyclodextrin and the abundant oxygen containing hydroxyl groups of FAH. The adsorption isotherm was properly fitted to the Langmuir adsorption model to denote the monolayer adsorption and maximum adsorption capacity of adsorbent was calculated to be 185.52 mg g^{-1} . The pseudo-second order model demonstrates the adsorption mechanism can be ascribed to the electrostatic interactions on the boundary layer of FAH-rGO/CD-4 on removal of As (V). The coexisting phosphate and bicarbonate ions reduce the adsorption rate of As (V) removal compared than other anions. The regeneration study of as-prepared composites declare that the materials can be easily reused up to five consecutive cycles without significant loss in removal efficiency. Thus, the novel FAH-rGO/CD nanocomposite proves to be a potential adsorbent for As (V) removal.

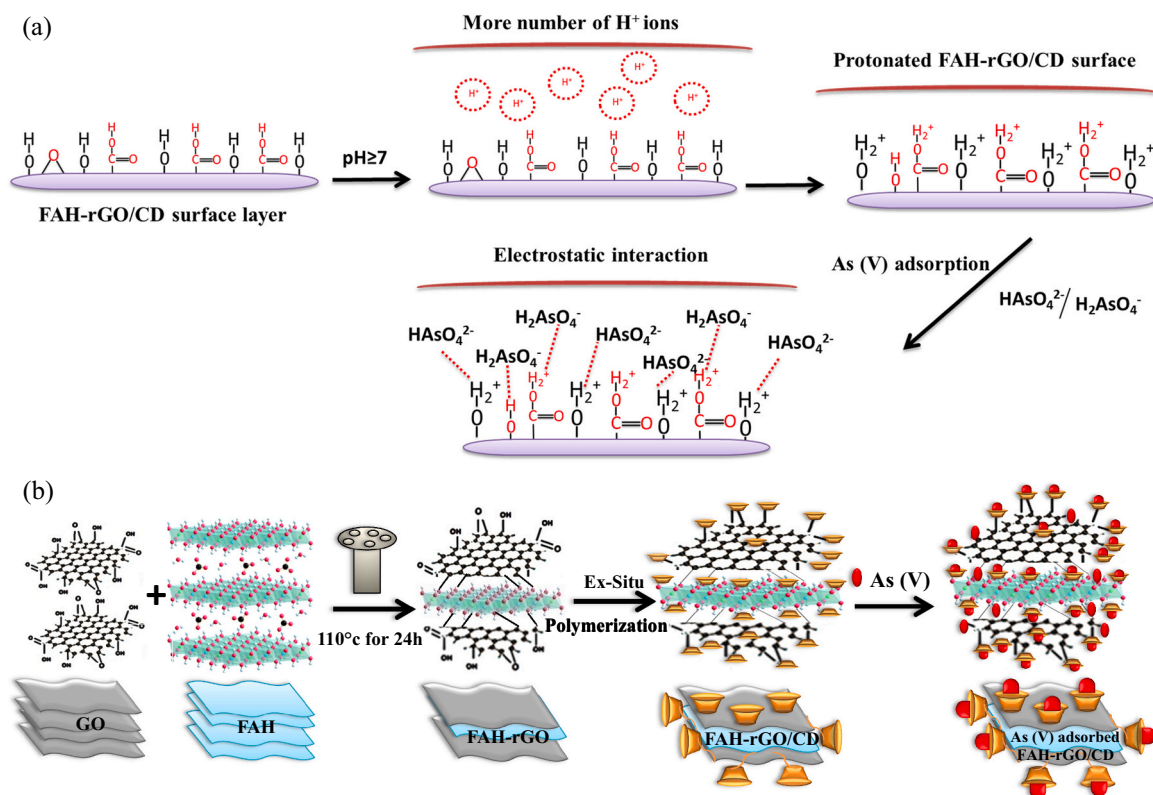


Fig. 13. (a) Schematic illustration of possible interaction between FAH-rGO/CD and As(V) ions, Schematic illustration of As(V) adsorption by FAH-rGO/CD.

Table 4
Comparative studies of various LDH/GO/ β -CD adsorbents on As(V) removal.

Adsorbent material	Adsorption capacity (mg g^{-1})	pH	Reference
Graphene oxide/ferric hydroxide	23.78	4–7	[14]
Magnetite-partially reduced graphene oxide	131.9	4	[48]
Zn/Fe-LDH microspheres	85.7	–	[49]
Magnetite-graphene-LDH	73.14	8	[50]
Magnetic nanoparticle-supported layered double hydroxide nanocomposites	83.01	1–5	[51]
Cobalt-aluminum layered double hydroxide on boehmite surface	28.73	7	[52]
Magnetic nanoparticles decorated with β -cyclodextrin functionalized graphene oxide	99	6	[53]
Zero-valent iron impregnated chitosan carboxymethyl- β -cyclodextrin composite beads	13.51	6	[54]
β -Cyclodextrin assisted Fe-Al double layered hydroxide/reduced Graphene Oxide	185.52	7	This study

CRedit authorship contribution statement

We Acknowledge that, all the persons who have sufficiently participated in this work takes public responsibility for the content. The contribution made by each authors are as follows.

V. Nithya Priya: Conceptualization, Writing - original draft. **M. Rajkumar:** Supervision. **J. Mobika:** Formal analysis. **S.P Linto Sibi:** Writing - review & editing.

Declaration of Competing Interest

The authors declare that they have no known competing financial interests or personal relationships that could have appeared to influence the work reported in this paper.

References

- [1] D. Morillo, A. Uheida, G. Pérez, M. Muhammed, M. Valiente, Journal of colloid and interface science arsenate removal with 3-mercaptopropanoic acid-coated superparamagnetic iron oxide nanoparticles, J. Colloid Interface Sci. 438 (2015) 227–234, <https://doi.org/10.1016/j.jcis.2014.10.005>.
- [2] D. Morillo, G. Pérez, M. Valiente, Journal of colloid and Interface science efficient arsenic (V) and arsenic (III) removal from acidic solutions with novel forager sponge-loaded superparamagnetic iron oxide nanoparticles, 2015, J. Colloid Interface Sci. 453 (2015) 132–141, <https://doi.org/10.1016/j.jcis.2015.04.048>.
- [3] Y. Jeong, M. Fan, S. Singh, C.L. Chuang, B. Saha, J. Hans van Leeuwen, Evaluation of iron oxide and aluminum oxide as potential arsenic(V) adsorbents, Chem. Eng. Process. Intensif. 46 (10) (2007) 1030–1039, <https://doi.org/10.1016/j.ccep.2007.05.004>.
- [4] V.N. Priya, M. Rajkumar, G. Magesh, J. Mobika, S.P.L. Sibi, Chitosan assisted Fe-Al double layered hydroxide/reduced graphene oxide composites for As(V) removal, Mater. Chem. Phys. 251 (V) (2020), 123108 [j.matchemphys.2020.123108](https://doi.org/10.1016/j.materchemphys.2020.123108).
- [5] Y. Wang, W. Liu, T. Wang, J. Ni, Arsenate adsorption onto Fe-TNTs prepared by a novel water-ethanol hydrothermal method: mechanism and synergistic effect, J. Colloid Interface Sci. 440 (2015) 253–262, <https://doi.org/10.1016/j.jcis.2014.10>.
- [6] P.L. Smedley, et al., Arsenic associations in sediments from the loess aquifer of La Pampa, Argentina 20 (2005) 989–1016, <https://doi.org/10.1016/j.apgeochem.2004.10.005>.
- [7] S.R. Samadder, Impact of arsenic pollution on spatial distribution of human development index (July), J. Civil Eng. (2011), <https://doi.org/10.1007/s12205-011-1046-7>.
- [8] A. Senn, S.J. Hug, R. Kaegi, J.G. Hering, A. Voegelin, Arsenate co-precipitation with Fe(II) oxidation products and retention or release during precipitate aging Anna-Caterina, Water Res. 131 (2018) 334–345, <https://doi.org/10.1016/j.watres.2017.12.038>.
- [9] M. Zaw, M.T. Emmett, Arsenic removal from water using advanced oxidation processes 133 (2002) 113–118, [https://doi.org/10.1016/S0378-4274\(02\)00081-4](https://doi.org/10.1016/S0378-4274(02)00081-4).
- [10] R. Guell, C. Fontàs, V. Salvado, E. Antico, Modelling of liquid – liquid extraction and liquid membrane separation of arsenic species in environmental matrices 72 (2010) 319–325, <https://doi.org/10.1016/j.seppur.2010.02.023>.

- [11] X. Jiang, C. Peng, D. Fu, Z. Chen, L. Shen, Q. Li, T. Ouyang, Y. Wang, Removal of arsenate by ferrihydrite via surface complexation and surface precipitation, *Appl. Surf. Sci.* 353 (2015) 1087–1094, <https://doi.org/10.1016/j.apsusc.2015.06.190>.
- [12] P. Bahmani, A. Maleki, H. Daraei, M. Khamforoush, High-flux ultrafiltration membrane based on electrospun polyacrylonitrile nanofibrous scaffolds for arsenate removal from aqueous solutions, *J. Colloid Interface Sci.* 506 (2017) 564–571, <https://doi.org/10.1016/j.jcis.2017.07.086>.
- [13] S.P. Taegu, D.U. Choi, Arsenic (V) removal using an amine-doped acrylic ion exchange fiber : kinetic, equilibrium, and regeneration studies, *J. Hazard. Mater.* 5 (325) (2016), <https://doi.org/10.1016/j.jhazmat.2016.12.003>.
- [14] M. Pessoa Lopes, C.F. Galinha, J.G. Crespo, S. Velizarov, Optimisation of arsenate removal from water by an integrated ion-exchange membrane process coupled with Fe co-precipitation, *Sep. Purif. Technol.* 246 (2020), 116894, <https://doi.org/10.1016/j.seppur.2020.116894>.
- [15] K. Zhang, V. Dwivedi, C. Chi, J. Wu, Graphene oxide/ferric hydroxide composites for efficient arsenate removal from drinking water, *J. Hazard. Mater.* 182 (1–3) (2010) 162–168, <https://doi.org/10.1016/j.jhazmat.2010.06.010>.
- [16] X. He, X. Qiu, J. Chen, Colloids and surfaces A : physicochemical and engineering aspects preparation of Fe(II)-Al layered double hydroxides : application to the adsorption / reduction of chromium, *Colloids Surf. A Physicochem. Eng. Asp.* 516 (2017) 362–374, <https://doi.org/10.1016/j.colsurfa.2016.12.053>.
- [17] R. Justin, B. Chen, Characterisation and drug release performance of biodegradable chitosan – graphene oxide nanocomposites, *Carbohydr. Polym.* 103 (2014) 70–80, <https://doi.org/10.1016/j.carbpol.2013.12.012>.
- [18] L. Ai, C. Zhang, Z. Chen, Removal of methylene blue from aqueous solution by a solvothermal-synthesized graphene / magnetite composite, *J. Hazard. Mater.* 192 (3) (2011) 1515–1524, <https://doi.org/10.1016/j.jhazmat.2011.06.068>.
- [19] H. Rashidi Nodeh, W.A. Wan Ibrahim, I. Ali, M.M. Sanagi, Development of magnetic graphene oxide adsorbent for the removal and preconcentration of As(III) and As(V) species from environmental water samples, *Environ. Sci. Pollut. Res.* 23 (10) (2016) 9759–9773, <https://doi.org/10.1007/s11356-016-6137-z>.
- [20] I. Ali, O.M.L. Alharbi, A. Tkachev, E. Galunin, A. Burakov, V.A. Grachev, Water treatment by new-generation graphene materials: hope for bright future, *Environ. Sci. Pollut. Res.* 25 (8) (2018) 7315–7329, <https://doi.org/10.1007/s11356-018-1315-9>.
- [21] I. Ali, O.M.L. Alharbi, Z.A. Allothman, A. Alwarthan, Facile and eco-friendly synthesis of functionalized iron nanoparticles for cyanazine removal in water, *Colloids Surf. B Biointerfaces* 171 (2018) 606–613, <https://doi.org/10.1016/j.colsurfb.2018.07.071>.
- [22] I. Ali, Microwave assisted economic synthesis of multi walled carbon nanotubes for arsenic species removal in water: Batch and column operations, *J. Mol. Liq.* 271 (2018) 677–685, <https://doi.org/10.1016/j.molliq.2018.09.021>.
- [23] I. Ali, O.M.L. Alharbi, Z.A. Allothman, A.M. Al-Mohaimed, A. Alwarthan, Modeling of fenuron pesticide adsorption on CNTs for mechanistic insight and removal in water, *Environ. Res.* 170 (2019) 389–397, <https://doi.org/10.1016/j.envres.2018.12.066>.
- [24] I. Ali, et al., Graphene based adsorbents for remediation of noxious pollutants from wastewater, *Environ. Int.* (2019) 160–180, <https://doi.org/10.1016/j.envint.2019.03.029>.
- [25] I. Ali, O.M.L. Alharbi, Z.A. Allothman, A.Y. Badjah, A. Alwarthan, A.A. Basheer, Artificial neural network modeling of amido black dye sorption on iron composite nano material: kinetics and thermodynamics studies, *J. Mol. Liq.* 250 (2018) 1–8, <https://doi.org/10.1016/j.molliq.2017.11.163>.
- [26] A.A. Basheer, I. Ali, Stereoselective uptake and degradation of (±)-o,p-DDD pesticide stereoisomers in water-sediment system, *Chirality* 30 (9) (2018) 1088–1095, <https://doi.org/10.1002/chir.22989>.
- [27] N.H. Al-Shaalan, I. Ali, Z.A. Allothman, L.H. Al-Wahaibi, H. Alabdulmonem, High performance removal and simulation studies of diuron pesticide in water on MWCNTs, *J. Mol. Liq.* 289 (2019), 111039, <https://doi.org/10.1016/j.molliq.2019.111039>.
- [28] O.M.L. Ali, Z.A. Alharbi, A. Allothman, Alwarthan, A.M. Al-Mohaimed, Preparation of a carboxymethylcellulose-iron composite for uptake of atorvastatin in water, *Int. J. Biol. Macromol.* 132 (2019) 244–253, <https://doi.org/10.1016/j.ijbiomac.2019.03.211>.
- [29] I. Ali, H.Y. Aboul-Enein, Speciation of arsenic and chromium metal ions by reversed phase high performance liquid chromatography, *Chemosphere* 48 (3) (2002) 275–278, [https://doi.org/10.1016/S0045-6535\(02\)00085-1](https://doi.org/10.1016/S0045-6535(02)00085-1).
- [30] S.S.D. Elanchezhyan, S. Meenakshi, Synthesis and characterization of chitosan / Mg-Al layered double hydroxide composite for the removal of oil particles from oil-in-water emulsion, *Int. J. Biol. Macromol.* 104 (2017) 1586–1595, <https://doi.org/10.1016/j.ijbiomac.2017.01.095>.
- [31] G.B.B. Varadwaj, O.A. Oyetade, S. Rana, B.S. Martincigh, S.B. Jonnalagadda, V. O. Nyamori, Facile synthesis of three-dimensional Mg-Al layered double hydroxide/partially reduced graphene oxide nanocomposites for the effective removal of Pb²⁺ from Aqueous Solution, *ACS Appl. Mater. Interfaces* 9 (2017) 17290–17305, <https://doi.org/10.1021/acsami.6b16528>.
- [32] S. Lata, S.R. Samadder, Removal of arsenic from water using nano adsorbents and challenges : a review, *J. Environ. Manag.* 166 (2016) 387–406, <https://doi.org/10.1016/j.jenvman.2015.10.039>.
- [33] G.E. Adamov, K.S. Levchenko, V.R. Kurbangaleev, P.S. Shmelin, E.P. Grebennikov, Functional hybrid nanostructures for nanophotonics: synthesis, properties, and application, *Russ. J. General Chem.* 83 (11) (2013) 2195–2202, <https://doi.org/10.1134/S107036321311039X>.
- [34] S.K. Kumar, S. Jiang, Chitosan-functionalized graphene oxide : a novel adsorbent an efficient adsorption of arsenic from aqueous solution, *Biochem. Pharmacol.* (2016), <https://doi.org/10.1016/j.jece.2016.02.035>.
- [35] M. Wei, Selective adsorption of phenol and nitrobenzene by β -cyclodextrin-intercalated layered double hydroxide: equilibrium and kinetic study, *Chem. Eng. Technol.* (9) (2011) 1559–1566, <https://doi.org/10.1016/j.electacta.2012.07.071>.
- [36] L. Fan, C. Luo, M. Sun, H. Qiu, X. Li, Colloids and surfaces B : biointerfaces synthesis of magnetic β -cyclodextrin - chitosan / graphene oxide as nanoadsorbent and its application in dye adsorption and removal, *Colloids Surf. B Biointerfaces* 103 (2013) 601–607, <https://doi.org/10.1016/j.colsurfb.2012.11.023>.
- [37] M. Yusuf, M. Kumar, M.A. Khan, M. Sillanpa, H. Arafat, A review on exfoliation, characterization, environmental and energy applications of graphene and graphene-based composites, *Adv. Colloid Interface Sci.* 273 (2019), 102036, <https://doi.org/10.1016/j.cis.2019.102036>.
- [38] M. Yusuf, M.A. Khan, M. Otero, E.C. Abdullah, M. Hosomi, A. Terada, S. Riya, Journal of colloid and interface science synthesis of CTAB intercalated graphene and its application for the adsorption of AR265 and AO7 dyes from water, *J. Colloid Interface Sci.* 493 (2017) 51–61, <https://doi.org/10.1016/j.jcis.2017.01.015>.
- [39] A. Terada, S. Riya, A. Ahmad, Dodecyl sulfate chain anchored mesoporous graphene : synthesis and application to sequester heavy metal ions from aqueous phase, *Chem. Eng. J.* (2016), <https://doi.org/10.1016/j.cej.2016.06.109CEJ>.
- [40] W. Tungtittiplakorn, Engineered polymeric nanoparticles for bioremediation of hydrophobic contaminants, *Environ. Sci. Technol.* 39 (5) (2005) 1354–1358, <https://doi.org/10.1021/es049031a>.
- [41] W. Tungtittiplakorn, Engineered polymeric nanoparticles for soil remediation 38 (5) (2004) 1605–1610, <https://doi.org/10.1021/es0348997>.
- [42] M.S. Gasser, H.T. Mohsen, H.F. Aly, Colloids and surfaces A : physicochemical and engineering aspects humic acid adsorption onto Mg / Fe layered double hydroxide 331 (2008) 195–201, <https://doi.org/10.1016/j.colsurfa.2008.08.002>.
- [43] S.J. Palmer, R.L. Frost, T. Nguyen, Hydrotalcites and their role in coordination of anions in Bayer liquors : anion binding in layered double hydroxides 253 (2009) 250–267, <https://doi.org/10.1016/j.ccr.2008.01.012>.
- [44] R. Chitarkar, S. Tezuka, A. Sonoda, K. Ooi, T. Tomidab, Studies on selective adsorbents for oxo-anions. Nitrate ion-exchange properties of layered double hydroxides with different metal atoms, *Green Chem.* (2004) 104–109, <https://doi.org/10.1039/B314938M>.
- [45] N. Viswanathan, S. Meenakshi, Applied clay science selective fluoride adsorption by a hydrotalcite / chitosan composite, *Appl. Clay Sci.* 48 (4) (2010) 607–611, <https://doi.org/10.1016/j.clay.2010.03.012>.
- [46] M. Dinari, A. Haghghi, P. Asadi, Facile synthesis of ZnAl-EDTA layered double hydroxide/poly(vinyl alcohol) nanocomposites as an efficient adsorbent of Cd(II) ions from the aqueous solution, *Appl. Clay Sci.* 170 (2019) 21–28, <https://doi.org/10.1016/j.clay.2019.01.007>.
- [47] O. Rahmanian, M. Dinari, S. Neamati, Synthesis and characterization of citrate intercalated layered double hydroxide as a green adsorbent for Ni²⁺ and Pb²⁺ removal, *Environ. Sci. Pollut. Res.* 25 (36) (2018) 36267–36277, <https://doi.org/10.1007/s11356-018-3584-8>.
- [48] J.A. Bobb, F.S. Awad, S. Moussa, M.S. El-Shall, Laser synthesis of magnetite-partially reduced graphene oxide nanocomposites for arsenate removal from water, *J. Mater. Sci.* 55 (13) (2020) 5351–5363, <https://doi.org/10.1007/s10853-020-04363-6>.
- [49] X. Dai, S. Zhang, G.L.N. Waterhouse, H. Fan, S. Ai, Recyclable polyvinyl alcohol sponge containing flower-like layered double hydroxide microspheres for efficient removal of As(V) anions and anionic dyes from water, *J. Hazard. Mater.* 367 (2019) 286–292, <https://doi.org/10.1016/j.jhazmat.2018.12.092>.
- [50] X.L. Wu, L. Wang, C.L. Chen, A.W. Xu, X.K. Wang, Water-dispersible magnetite-graphene-LDH composites for efficient arsenate removal, *J. Mater. Chem.* 21 (43) (2011) 17353–17359, <https://doi.org/10.1039/c1jm12678d>.
- [51] S.H. Lee, H. Choi, K.W. Kim, Removal of As(V) and Sb(V) in water using magnetic nanoparticle-supported layered double hydroxide nanocomposites, *J. Geochem. Explor.* 184 (2018) 247–254, <https://doi.org/10.1016/j.gexplo.2016.11.015>.
- [52] S.Y. Lee, K.W. Jung, J.W. Choi, Y.J. Lee, In situ synthesis of hierarchical cobalt-aluminum layered double hydroxide on boehmite surface for efficient removal of arsenate from aqueous solutions: Effects of solution chemistry factors and sorption mechanism, *Chem. Eng. J.* 368 (2019) 914–923, <https://doi.org/10.1016/j.cej.2019.03.043>.
- [53] A.S.K. Kumar, S. Jiang, Synthesis of magnetically separable and recyclable magnetic nanoparticles decorated with β -cyclodextrin functionalized graphene oxide an excellent adsorption of As(V)/(III), *J. Mol. Liq.* 237 (3) (2017), <https://doi.org/10.1016/j.molliq.2017.04.093>.
- [54] M. Tajuddin Sikder, S. Tanaka, T. Saito, M. Kurasaki, Application of zerovalent iron impregnated Chitosan-carboxymethyl- β - cyclodextrin composite beads as arsenic sorbent, *J. Environ. Chem. Eng.* 2 (1) (2014) 370–376, <https://doi.org/10.1016/j.jece.2014.01.009>.
- [55] D. Lu, S. Lin, L. Wang, X. Shi, C. Wang, Y. Zhang, *Electrochimica Acta* Synthesis of cyclodextrin-reduced graphene oxide hybrid nanosheets for sensitivity enhanced electrochemical determination of diethylstilbestrol, *Electrochim. Acta* 85 (2012) 131–138, <https://doi.org/10.1016/j.electacta.2012.07.071>.
- [56] L. Li, L. Fan, M. Sun, H. Qiu, X. Li, H. Duan, C. Luo, Colloids and Surfaces B : Biointerfaces Adsorbent for chromium removal based on graphene oxide functionalized with magnetic cyclodextrin – chitosan, *Colloids Surf. B Biointerfaces* 107 (2013) 76–83, <https://doi.org/10.1016/j.colsurfb.2013.01.074>.
- [57] W. Hu, X. Wu, F. Jiao, W. Yang, Y. Zhou, Preparation and characterization of magnetic Fe₃O₄ @ sulfonated β -cyclodextrin intercalated layered double hydroxides for methylene blue removal 3994 (2016), <https://doi.org/10.1080/19443994.2016.1155173>.
- [58] L. Hu, W. Gao, J. He, H. Liu, B. Li, X. Zhang, Ni-Ti-layered double hydroxide intercalated with β -CD and CM- β -CD : interaction between the interlayer guests and

- the laminates, *J. Mol. Struct.* 1041 (2013) 151–155, <https://doi.org/10.1016/j.molstruc.2013.03.019>.
- [59] M. Dinari, S. Neamati, Surface modified layered double hydroxide/polyaniline nanocomposites: synthesis, characterization and Pb²⁺ removal, *Colloids Surf. A Physicochem. Eng. Asp.* 589 (2020), 124438, <https://doi.org/10.1016/j.colsurfa.2020.124438>.
- [60] K. Zargoosh, S. Kondori, M. Dinari, S. Mallakpour, Synthesis of layered double hydroxides containing a biodegradable amino acid derivative and their application for effective removal of cyanide from industrial wastes, *Ind. Eng. Chem. Res.* 54 (3) (2015) 1093–1102, <https://doi.org/10.1021/ie504064k>.
- [61] O. Rahmanian, S. Amini, M. Dinari, Preparation of Zinc/iron Layered Double Hydroxide Intercalated by Citrate Anion for Capturing Lead (II) from Aqueous Solution, *Elsevier B.V.*, 2018, <https://doi.org/10.1016/j.molliq.2018.02.018>.
- [62] Y. Lu, et al., An investigation of ultrathin nickel-iron layered double hydroxide nanosheets grown on nickel foam for high-performance supercapacitor electrodes 714 (2017) 63–70, <https://doi.org/10.1021/acsam.9b02055>.
- [63] P. Bhawal, S. Ganguly, T.K. Chaki, N.C. Das, RSC advances synthesis and characterization of graphene oxide filled ethylene methyl acrylate hybrid nanocomposites, *RSC Adv.* 6 (2016) 20781–20790, <https://doi.org/10.1039/C5RA24914G>.
- [64] M. Srivastava, J. Singh, M. Yashpal, D.K. Gupta, R.K. Mishra, S. Tripathi, A.K. Ojha, Synthesis of superparamagnetic bare Fe₃O₄ nanostructures and core / shell (Fe₃O₄ / alginate) nanocomposites, *Carbohydr. Polym.* 89 (3) (2012) 821–829, <https://doi.org/10.1016/j.carbpol.2012.04.016>.
- [65] T. Esfandiari, N. Nasirizadeh, M. Dehghani, M.H. Ehrampoosh, Graphene oxide based carbon composite as adsorbent for Hg removal: Preparation, characterization, kinetics and isotherm studies, *Chin. J. Chem. Eng.* 25 (9) (2017) . 1170–1175, <https://doi.org/10.1016/j.cjche.2017.02.006>.
- [66] L. Jiang, Y. Liu, S. Liu, X. Hu, G. Zeng, X. Hu, S. Liu, S. Liu, B. Huang, M. Li, Fabrication of β -Cyclodextrin/poly (L-glutamic acid) supported magnetic graphene oxide and its adsorption behavior for 17 β -estradiol, *Chem. Eng. J.* 308 (2017) 597–605, <https://doi.org/10.1016/j.cej.2016.09.067>.
- [67] T. Wen, X. Wu, X. Tan, X. Wang, A. Xu, One-pot synthesis of water-swellaable Mg–Al layered double hydroxides and graphene oxide nanocomposites for efficient removal of As(V) from aqueous solutions, *Am. Chem. Soc.* (2013), <https://doi.org/10.1021/am4003556>.
- [68] M. Dinari, R. Tabatabaiean, Ultra-fast and highly efficient removal of cadmium ions by magnetic layered double hydroxide/guar gum bionanocomposites, *Carbohydr. Polym.* 192 (2018) 317–326, <https://doi.org/10.1016/j.carbpol.2018.03.048>.
- [69] M. Dinari, A. Haghghi, Ultrasound-assisted synthesis of nanocomposites based on aromatic polyamide and modified ZnO nanoparticle for removal of toxic Cr(VI) from water, *Ultrason. Sonochem.* 41 (2018) 75–84, <https://doi.org/10.1016/j.ultsonch.2017.09.023>.
- [70] M. Dinari, M. Hatami, Novel N-riched crystalline covalent organic framework as a highly porous adsorbent for effective cadmium removal, *J. Environ. Chem. Eng.* 7 (1) (2019), 102907, <https://doi.org/10.1016/j.jece.2019.102907>.
- [71] M. Dinari, M.A. Shirani, M.H. Maleki, R. Tabatabaiean, Green cross-linked bionanocomposite of magnetic layered double hydroxide/guar gum polymer as an efficient adsorbent of Cr(VI) from aqueous solution, *Carbohydr. Polym.* 236 (February) (2020), 116070, <https://doi.org/10.1016/j.carbpol.2020.116070>.
- [72] P. Wu, et al., Journal of Environmental Chemical Engineering Enhanced arsenate removal performance of nanostructured goethite with high content of surface hydroxyl groups, *Biochem. Pharmacol.* 2 (4) (2014) 2312–2320, <https://doi.org/10.1016/j.jece.2014.10.010>.
- [73] T. Lv, W. Ma, G. Xin, R. Wang, J. Xu, D. Liu, F. Liu, D. Pan, Physicochemical characterization and sorption behavior of Mg-Ca-Al(NO₃)₃ hydrotalcite-like compounds toward removal of fluoride from protein solutions, *J. Hazard. Mater.* 237–238 (3) (2012) 121–132, <https://doi.org/10.1016/j.jhazmat.2012.08.014>.
- [74] N. Inchaurredo, et al., Synthesis and adsorption behavior of mesoporous alumina and Fe-doped alumina for the removal of dominant arsenic species in contaminated waters, *Biochem. Pharm.* (2019), 102901, <https://doi.org/10.1016/j.jece.2019.102901>.
- [75] S. Mandal, M.K. Sahu, R. Kishore, Adsorption studies of arsenic (III) removal from water by zirconium polyacrylamide hybrid, *Water Resour. Ind.* 4 (2013) 51–67, <https://doi.org/10.1016/j.wri.2013.09.003>.
- [76] M. Dinari, R. Soltani, G. Mohammadnezhad, Kinetics and thermodynamic study on novel modified-mesoporous silica MCM-41/Polymer matrix nanocomposites: effective adsorbents for trace CrVI removal, *J. Chem. Eng. Data* 62 (8) (2017) 2316–2329, <https://doi.org/10.1021/acs.jced.7b00197>.